

ZeroGrads: Learning Local Surrogates for Non-Differentiable Graphics

MICHAEL FISCHER, University College London, United Kingdom

TOBIAS RITSCHEL, University College London, United Kingdom



Fig. 1. Our method optimizes arbitrary (black-box) graphics pipelines, which all do not trivially provide gradients, such as rendering (left: finding the box and light position under a discontinuous integrand), modelling (middle: discrete number of vertical and horizontal wicker stakes), and animation (right: optimal control of the engine turn-off time), by fitting a neural network to the loss landscape and then using the network’s gradients for parameter optimization.

Gradient-based optimization is now ubiquitous across graphics, but unfortunately can not be applied to problems with undefined or zero gradients. To circumvent this issue, the loss function can be manually replaced by a “surrogate” that has similar minima but is differentiable. Our proposed framework, *ZeroGrads*, automates this process by learning a neural approximation of the objective function, which in turn can be used to differentiate through arbitrary black-box graphics pipelines. We train the surrogate on an actively smoothed version of the objective and encourage locality, focusing the surrogate’s capacity on what matters at the current training episode. The fitting is performed online, alongside the parameter optimization, and self-supervised, without pre-computed data or pre-trained models. As sampling the objective is expensive (it requires a full rendering or simulator run), we devise an efficient sampling scheme that allows for tractable run-times and competitive performance at little overhead. We demonstrate optimizing diverse non-convex, non-differentiable black-box problems in graphics, such as visibility in rendering, discrete parameter spaces in procedural modelling or optimal control in physics-driven animation. In contrast to other derivative-free algorithms, our approach scales well to higher dimensions, which we demonstrate on problems with up to 35k interlinked variables.

CCS Concepts: • **Computing methodologies** → **Rendering**.

Additional Key Words and Phrases: Differentiable Rendering; Inverse Rendering; Surrogate Learning; Gradient Descent; Optimization

ACM Reference Format:

Michael Fischer and Tobias Ritschel. 2024. ZeroGrads: Learning Local Surrogates for Non-Differentiable Graphics. *ACM Trans. Graph.* 43, 4, Article 49 (July 2024), 15 pages. <https://doi.org/10.1145/3658173>

Authors’ addresses: Michael Fischer, University College London, United Kingdom, m.fischer@cs.ucl.ac.uk; Tobias Ritschel, University College London, United Kingdom, t.ritschel@ucl.ac.uk.

Permission to make digital or hard copies of part or all of this work for personal or classroom use is granted without fee provided that copies are not made or distributed for profit or commercial advantage and that copies bear this notice and the full citation on the first page. Copyrights for third-party components of this work must be honored. For all other uses, contact the owner/author(s).

© 2024 Copyright held by the owner/author(s).

0730-0301/2024/7-ART49

<https://doi.org/10.1145/3658173>

1 INTRODUCTION

Gradient-based optimization has recently become an essential part of many graphics applications, ranging from rendering to find light or reflectance [Fischer and Ritschel 2022a; Gardner et al. 2019; Rainer et al. 2019], over procedural material modelling [Hu et al. 2022a] to animation of characters or fluids [Habermann et al. 2021; Schenck and Fox 2018]. These methods provide state-of-the-art results, in particular when combined with large amounts of training data and neural networks (NNs) that represent the desired mappings or assets. In order to train these methods via gradient descent (GD), the pipeline needs to be fully differentiable, allowing to backpropagate gradients from the objective function to the optimization parameters. This often is enabled by intricate, task-specific derivations [Li et al. 2018; Loubet et al. 2019] or requires fundamental changes to the pipeline, such as the switch to a dedicated programming language [Bangaru et al. 2023, 2021; Hu et al. 2019; Jakob et al. 2022a].

In practice, the application of these ideas remains limited, as many existing graphics pipelines are black-boxes (e.g., entire 3D modelling packages such as Blender or rendering pipelines such as Renderman [Christensen et al. 2018] or Unity [Haas 2014]) that do not provide access to their internal workings and hence cannot be differentiated. Further, even if we were given access to the pipeline’s internals, the employed functions might not be differentiable (e.g., the step function) or provide gradients that are insufficient for convergence [Metz et al. 2021]. The mindset of this article is that we only have access to a forward model, e.g., a modeling pipeline, and a reference, e.g., a target image. Using these two, a loss can be computed – its gradients, however, cannot be used.

If a loss is not differentiable in practice, it can be approximated by a “surrogate” loss (Fig. 2). The surrogate is a function that has similar minima as the true loss, but also provides gradients that are useful when employed in an optimization. While the concept of surrogate modelling is not new (see Sec. 2), it remains unclear how to efficiently find a surrogate loss for any arbitrary graphics

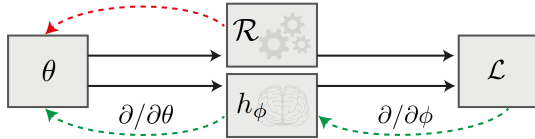


Fig. 2. Regular forward models \mathcal{R} might not be able to provide gradients w.r.t. their input parameters θ (red arrow, top). Our approach, ZeroGrads, provides this ability via a local learned surrogate h (green arrows, bottom) that maps θ to the associated loss and can be differentiated analytically.

pipeline, as here the sampling must be sparse (recall, rendering a sample is expensive), and the optimization problems’ dimensionality can vary by several orders of magnitude. In this article, we propose *ZeroGrads*, a systematic and efficient way of learning local surrogate losses, requiring no more than a forward model and a reference.

To learn our surrogate loss and use it in an optimization, we follow four key steps: We first smooth the original loss by convolving the cost landscape with a blur kernel, so that it provides gradients that lead to (improved) convergence when used during optimization. We secondly fit a surrogate, a parametric function such as a neural network or a quadratic potential, to that smoothed loss. As the surrogate is differentiable by construction, we can query it to get *surrogate gradients* that drive the parameter optimization. We thirdly constrain this fit to the local neighbourhood of the current parameters, as the global cost landscape is in large parts irrelevant for the current optimization step. By locally updating our surrogate, we allow it to focus on what matters “around” the current solution. However, querying the objective function to create samples for our surrogate fitting is expensive, as each sample requires the execution of the full forward model, such as a light transport simulation or physics solver. Therefore, fourth and finally, we derive an efficient sampler that reduces the variance of the surrogate’s gradient estimates and thus allows us to use ZeroGrads with a low number of sparse samples at tractable runtimes.

In contrast to prior work [Hu et al. 2022b], our local surrogate losses can be trained *online*, alongside the actual parameter optimization, and *self-supervised*, without the need for pre-trained models or pre-computed ground truth gradients. Moreover, in comparison to other gradient estimation techniques [Fischer and Ritschel 2022b; Spall 1992], our neural proxy allows us to move the noise and variance in the gradient estimates from the *parameter* domain into the *proxy* domain, where it is naturally smoothed by the network’s hysteresis, allowing ZeroGrads to scale up to very high dimensions. In summary, our contributions are:

- ZeroGrads, a framework that maps a forward model without usable gradients into a smooth, differentiable surrogate function, such as an NN, with analytic gradients.
- Reducing the variance of surrogate and parameter updates to allow tractable runtimes and unsupervised and successful on-the-fly optimization.
- Optimizing several non-differentiable black-box graphics problems from rendering (visibility) over modelling (discrete procedurals) to simulation and animation (optimal control).

- Showing that our surrogates scale favourably to higher dimensions, with up to several thousand correlated optimization variables, where existing derivative-free methods often struggle to converge.
- A publicly available implementation of our method and benchmarks at <https://github.com/mfischer-ucl/zerograds>

We would like to emphasize that we do not claim superiority (less variance, better convergence, ...) over existing, specialized methods such as Mitsuba [Jakob et al. 2022b], Redner [Li et al. 2018] or PhiFlow [Holl et al. 2020], but rather broaden the toolkit of inverse graphics solvers by now enabling gradient-based optimization on arbitrary, non-differentiable graphics pipelines.

2 PREVIOUS WORK

Optimization in Graphics. Parameters of graphics models are now routinely optimized so as to fulfill user-provided goals. The two main ingredients enabling this are gradient-based optimization and tunable architectures. We will not consider the many different exciting architectures in this work, but focus on the optimization itself. Gradients are typically computed by using a language that allows efficient auto-differentiation, such as PyTorch [Paszke et al. 2017] or JAX [Bradbury et al. 2018], often targeting GPUs. Unfortunately, several problems in graphics are not differentiable.

Gradient-free optimization algorithms [Rios and Sahinidis 2013] such as asking a user [Marks et al. 1997], global optimization [Jones et al. 1998], direct search [Powell 1994], simulated annealing (SA) [Kirkpatrick et al. 1983], simultaneous perturbation stochastic approximation (SPSA) [Spall 1992], particle swarms [Parsopoulos and Vrahatis 2002] or genetic algorithms (GAs) [Holland 1973] have largely fallen from favour in everyday graphics use. This is partially due to the fact that gradient-free optimization – even on smooth problems – often requires a large number of function evaluations before converging [Jamieson et al. 2012], and, in general, struggles with convergence as problem dimensionality increases. Additionally, gradient-free optimizers often suffer from high per-iteration cost in higher dimensions (e.g., finite differences (FD) or [Zhang et al. 2020], see Tab. 1), require the computation of the Hessian matrix in Newton-type methods, or make use of covariance-matrices (CMA-ES [Hansen 2016]), whose memory requirements grow quadratically with problem dimension and require computationally complex steps like inversion or eigendecomposition. The aforementioned aspects often lead to trade-offs between performance, scalability and runtime that practitioners have to take into consideration. GD, in contrast, has strong convergence guarantees (under convex objectives), is highly scalable, can be parallelized effectively, and has shown superior performance in high-dimensional settings (e.g., NN training). Unfortunately, it cannot be used on many relevant problems (although the cost landscape itself might be smooth), as many graphics pipelines are simply not designed to be differentiable. Our approach circumvents this issue by fitting a model of the cost landscape, which can then be differentiated to provide *surrogate* gradients that GD can work with. Even for non-smooth problems, our formulation makes the problem smooth and hence amenable to GD.

Table 1. Comparison of optimization algorithms. n is the problem dimensionality, p is the population size in evolutionary algorithms, k is the state’s size in stateful algorithms, b is the batchsize in multi-sample algorithms, t and t_i are the times required for a function evaluation and a state update, respectively. Stateful denotes whether the method maintains a state other than the current optimization parameter.

	Memory	Gradient	Iter. Cost	Scalable	Robust	Stateful
Ours	$n + k$	✓	$b \cdot t + t_{GD}$	✓	✓	✓
SPSA	n	✓	$2t$	✓	✓	×
FR22	n	✓	$b \cdot t$	✓	?	×
CMA-ES	$n^2 + k$	×	$p \cdot t + t_{CMA}$	✓	✓	✓
GA	n	×	$p \cdot t + t_{GA}$	×	×	✓
FD	n	✓	$2n \cdot t$	×	×	×
SA	n	×	t	×	×	×

Differentiation. Most graphics pipelines used in production (e.g., Blender, GIMP, Photoshop) are not differentiable, as they are not implemented in a differentiable programming language. The deeper underlying mathematical problem is that their output often relies on integration – however, differentiation and the typical integral estimation through Monte Carlo (MC) cannot be interchanged without further considerations. A prominent example are discontinuities in rendering, which have sparked a body of work by Bangaru et al. [2021]; Kato et al. [2018]; Lee et al. [2018]; Li et al. [2018]; Liu et al. [2019]; Loper and Black [2014]; Rhodin et al. [2015]; Xing et al. [2022] or Loubet et al. [2019], to only name a few salient ones. Similar problems appear in vector graphics [Li et al. 2020], signed distance functions (SDFs) [Bangaru et al. 2022; Vicini et al. 2022], entire programs [Chandra et al. 2022] or physics [Chang et al. 2016; Hu et al. 2019; Mrowca et al. 2018]. All these approaches require access to the internals of the graphics pipeline in order to replace or change parts such that gradients can be backpropagated. Our approach, in contrast, assumes the pipeline to be a black-box and does not make any assumptions or approximations to the internals.

Gradient Smoothing. Another approach for optimizing non-differentiable problems has been proposed as *stochastic* optimization. Here, discontinuities and plateaus are smoothed out by optimizing over the expected value of a distribution (generally MC-approximation via randomized sampling) instead of a rigid parameter [Berthet et al. 2020; Chaudhuri and Solar-Lezama 2010; Duchi et al. 2012; Staines and Barber 2013], with the resulting gradient sometimes being referred to as *zeroth-order* [Suh et al. 2022b]. This has successfully been used to smooth out plateaus and discontinuities in rendering ([Fischer and Ritschel 2022b; Le Lidec et al. 2021]), contact dynamics in robotics ([Montaut et al. 2023; Suh et al. 2022a]) and policy optimization in reinforcement learning ([Suh et al. 2022b; Williams 1992]), albeit without the explicit learning of a proxy cost model.

Proxies. A key insight is that we only need the loss’ gradients, and not those of the entire pipeline. Hence, if a part in a conventional graphics pipeline cannot be differentiated, we search for a similar function that we can differentiate instead, our *proxy*. As the proxy is an analytic function, the gradients w.r.t. its input can readily be computed via automatic differentiation (AD) and then be used for

optimization. Graphics is a good fit for neural proxies, as we can freely sample the objective in many cases, e.g., by rendering an image or running a simulation (a “simulation-optimization” setting [Law et al. 2007]). While easy to do, creating a sample is expensive.

The concept of “Neural Proxies” was pioneered for physics by Grzeszczuk et al. [1998] and is now applied to problems such as material editing [Hu et al. 2022a], photo editing [Fischer et al. 2020; Tseng et al. 2022], hardware and design [Tseng et al. 2019], software synthesis [Esmailzadeh et al. 2012], simulation [Ansari et al. 2022; Munk et al. 2019; Renda et al. 2020] or animation [Navrátil et al. 2019; Shirobokov et al. 2020; Sin et al. 2021]. Rendering itself becomes differentiable when replaced by a NN proxy [Nalbach et al. 2017], however, having a NN emulate the complex behaviour of a full graphics pipeline might not scale to complex assets.

Surrogate losses. Surrogate losses [Queipo et al. 2005] (sometimes also called meta-models [Barton 1994; Box and Draper 1987]) extend the idea of proxies by providing an approximation to the *entire* forward model’s behaviour by only emulating its response (or loss landscape), without necessarily replicating all the internals of the model. Differentiating the surrogate will provide gradients which can then be used for (gradient-based) optimization. Surrogates are especially popular when taking a sample is expensive, like in airplane design [Forrester and Keane 2009] or neural architecture search [Zhou et al. 2020], and can be modelled in a number of ways, e.g., through polynomials [Jones et al. 1998], radial basis functions (RBFs) [Gutmann 2001] and recently neural networks [Grabocka et al. 2019; Patel et al. 2020]. Most of these methods learn surrogates for the entire cost landscape (typically in a simplified setting, e.g., classification), with the exception of response surface maps (RSMs), which fit a first- or second order polynomial to the local neighbourhood, but are known to not converge on higher-dimensional problems [Wan et al. 2005]. More crucially, aside from global fitting, most methods assume the availability of a large set of data samples, e.g., a curated image collection like ImageNet [Deng et al. 2009]. In our setting, in contrast, sampling is expensive, which is why we sample *sparsely and locally* and fit the surrogate in-the-loop, during optimization. Our method hence extends the family of surrogate-based optimizers, and, in contrast to previous work, scales to a wide range of optimization tasks in high dimensions.

Gradient estimation. The surrogate itself is updated gradient-based, by sampling the objective function a finite number of times and then estimating the surrogate’s gradient from its prediction error. For general learning, building gradients is fundamentally a MC estimation problem [Mohamed et al. 2020], akin to what graphics routinely is solving for rendering [Veach 1998]. We identify the similarity of estimating proxy gradients and simulating light transport (high dimensionality, sparsity, product integrands) and employ variance reduction based on importance sampling [Kahn 1950; Kajiya 1986; Veach 1998] the local parameter neighbourhood to increase the efficiency of our surrogate gradient estimates.

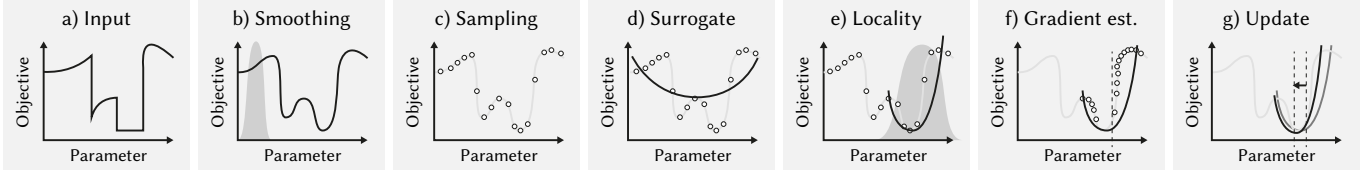


Fig. 3. A conceptual illustration of our approach; each subplot shows a one-dimensional cost landscape. For details please refer to Sec. 3: Overview.

3 OUR APPROACH

Given a scalar objective function $f(\theta) : \Theta \rightarrow \mathbb{R}_0^+$ over an n -dimensional parameter space Θ , we would like to find the optimal parameters θ^* that minimize f . Typically, gradient-based optimizers such as SGD or ADAM are used for such a task. However, in the setting of this work, their direct use is not possible, as the objective’s gradients $\partial f / \partial \theta$ are either not accessible (in a black-box pipeline), undefined (at discontinuities), zero (on a plateau) or too costly to compute (e.g., when appearing in an integral). We are, however, able to sample this objective function by sampling a set of parameters and then comparing the resulting output with the reference. We propose to now *locally* fit a tunable and differentiable surrogate function $h(\theta, \phi)$ to those samples, whose derivative $\partial h / \partial \theta$ will act as *surrogate gradient* and drive the optimization.

Overview. Our approach is summarized in Alg. 1 and Fig. 3. Given an arbitrary (potentially non-smooth and non-convex) objective function (Fig. 3a, also called loss landscape) and a randomly initialized parameter state θ , we first smooth the objective via convolution with a Gaussian kernel in order to reduce plateaus (Sec. 3.1 and Fig. 3b). We subsequently fit our surrogate h (Sec. 3.2) to this smooth objective. However, sampling is expensive (requiring a full rendering or simulator run), and global sampling and surrogate fitting would be very approximate (Fig. 3c, d), which is why we enforce locality via another Gaussian kernel (Fig. 3e and Sec. 3.3) and hence encourage the surrogate to focus on what matters at the current optimization iteration. Unfortunately, we do not have supervision gradients to train our surrogate on, which is why we must estimate the surrogate’s gradient (Sec. 3.4). While some samples are more informative than others, it is unclear how to find those, i.e., how we can efficiently sample this convolved space. To this end, we derive an efficient importance-sampler (Fig. 3f and Sec. 3.5) that samples according to the locality terms and thus reduces the variance of the estimated surrogate gradient. Finally, we use this estimated gradient to update our surrogate (Fig. 3g) in order to improve its fit to the objective. We can then descend along the surrogate’s gradient $\partial h / \partial \theta$ (readily available via AD) to update the optimization parameter θ and repeat the process from b) onward, i.e., the surrogate is updated from its previous state instead of re-fit. Lines 5 and 6 in Alg. 1 illustrate this, where OPTIMIZE performs gradient descent steps on a variable.

3.1 Smooth objective

As the objective might not always be differentiable (or provide gradients that are of little use [Metz et al. 2021]), we seek to find a function that has similar optima and is differentiable. In practice, the issue is not so much in non-differentiable point singularities (which

are even present in the popular ReLU activation), but regions with zero gradients (“plateaus”). These can be removed by convolving the objective with a blur kernel. Similar ideas have been applied to rasterization [Liu et al. 2019; Petersen et al. 2022] and path-tracing [Fischer and Ritschel 2022b], which we scale to arbitrary spaces. We define the smooth objective $g(\theta) : \Theta \rightarrow \mathbb{R}_0^+$ as

$$g(\theta) = \kappa * f(\theta) = \int_{\Theta} \kappa(\tau) f(\theta - \tau) d\tau, \quad (1)$$

a convolution of the objective f and a smoothing kernel κ , which we choose to be a Gaussian. Convolution with a Gaussian kernel has several desirable properties, e.g., convexity is preserved, it holds that $L_g \leq L_f$, i.e., the smooth objective is stronger Lipschitz-bound than f , and the gradient ∇_g is Lipschitz-continuous even when ∇_f is not [Nesterov and Spokoiny 2017], as is the case on many of our problems (e.g., Fig. 3a)). We show visualizations of Eq. 1 in Fig. 5.

3.2 Surrogate

The key ingredient, the surrogate $h(\theta, \phi) : \Theta \times \Phi \rightarrow \mathbb{R}_0^+$, consumes θ (like f and g , which it emulates), but also takes the tunable parameters ϕ from the m -dimensional surrogate parameter space Φ .

We encode our surrogate in a differentiable proxy function of variable form, which can take the form of polynomials, RBFs or NNs (see Sec. 4.4 for examples) and whose analytic parametrization allows to easily get the surrogate gradient $\partial h / \partial \phi$ and the parameter gradient $\partial h / \partial \theta$ via automatic differentiation. In contrast to linear methods (e.g., [Fischer and Ritschel 2022b; Spall 1992; Zhang et al. 2020]), our continuous surrogate formulation allows us to perform one or more gradient descent steps on the surrogate and to evaluate the estimated loss surface at a new position without re-running the forward model.

Algorithm 1 High-level pseudo-code of ZeroGrads.

Input: objective f , surrogate h

Output: optimized parameters θ minimizing f

```

1: procedure ZEROGRADS( $f, h$ )
2:    $\phi := \text{INIT}()$  ▷ surrogate parameters
3:    $\theta := \text{UNIFORM}()$  ▷ optimization parameters
4:   for  $i$  do
5:      $\phi = \text{OPTIMIZE}_1(\phi, \text{ESTIMATEGRADIENT}(\phi, \theta, f, h))$ 
6:      $\theta = \text{OPTIMIZE}_2(\theta, \partial h / \partial \theta)$ 
7:   end for
8:   return  $\theta$ 
9: end procedure

```

3.3 Localized surrogate loss

Matching h to g across the entire domain Θ might be too ambitious and furthermore is unnecessary, as most first-order gradient-based optimizers only ever query values at or around the current parameter θ . Instead, we create a surrogate that is focused around the current parameters by locally sampling the objective function.

The loss of the surrogate parameters ϕ “around” θ hence is

$$l(\theta, \phi) = \int_{\Theta} \lambda(\rho, \theta) (g(\rho) - h(\rho, \phi))^2 d\rho, \quad (2)$$

where λ is a weighting function that chooses how much context is considered around the current solution and ρ is from the parameter space Θ . We again choose a Gaussian with mean θ here, which is not to be confused with the smoothing kernel κ . Eq. 2 illustrates how the surrogate never has access to the gradients of the true objective – these might not even exist –, but learns self-supervised by only sampling the (smoothed) loss g .

3.4 Estimator

Combining the smoothed loss in Eq. 1 and the localized surrogate loss in Eq. 2, we arrive at the following expression:

$$l(\theta, \phi) = \int_{\Theta} \lambda(\rho, \theta) \underbrace{\left(\left[\int_{\Theta} \kappa(\tau) f(\rho - \tau) d\tau \right] - h(\rho, \phi) \right)^2}_{=: I(\rho, \phi)} d\rho. \quad (3)$$

We are now interested in the gradient of this expression w.r.t. the surrogate parameters ϕ , i.e.,

$$\frac{\partial}{\partial \phi} l(\theta, \phi) = \frac{\partial}{\partial \phi} \int_{\Theta} I(\rho, \phi) d\rho = \int_{\Theta} \frac{\partial}{\partial \phi} I(\rho, \phi) d\rho. \quad (4)$$

The above equality holds, according to Leibniz’ rule of differentiation under the integral sign, if, and only if, the integrand is continuous in ϕ and ρ [Li et al. 2018]. Our Gaussian locality weight λ fulfills this and $h(\rho, \phi)$ is continuous by definition, as it is a NN or quadratic potential. Through our previously introduced convolution (Eq. 1), the – originally discontinuous – objective f becomes smooth and hence leads to the inner integral being continuous in ρ . Leveraging the fact that a composition of continuous functions also is continuous, we can say that $I(\rho, \phi)$ is continuous in ϕ and hence use Eq. 4 as our gradient estimator:

$$\frac{\partial}{\partial \phi} l = \int_{\Theta} \frac{\partial}{\partial \phi} \lambda(\rho, \theta) \left(\left[\int_{\Theta} \kappa(\tau) f(\rho - \tau) d\tau \right] - h(\rho, \phi) \right)^2 d\rho \quad (5)$$

$$= \int_{\Theta} 2\lambda(\rho, \theta) \frac{\partial h(\rho, \phi)}{\partial \phi} \left(h(\rho, \phi) - \int_{\Theta} \kappa(\tau) f(\rho - \tau) d\tau \right) d\rho. \quad (6)$$

Here, the inner integral over τ is conditioned on the outer variable ρ , leading to a nested integration problem. A general, unbiased solution would estimate the inner and outer integrals with N and M samples, respectively, where $M \propto N$, leading to quadratic complexity. However, in this special case the function acting on the inner integral is linear, and the nested estimator thus remains unbiased even for constant N (see [Rainforth et al. 2018], Sec. 5 & Fig. 2).

We now aim to re-arrange Eq. 6 into a double-integral of a product, a form that is reliably solvable by the well-known approaches that

Algorithm 2 Estimating the surrogate’s gradient

Input: surrogate parameters ϕ , optimization parameter θ , objective f , surrogate h

Output: surrogate gradient $\nabla \phi$

```

1: procedure ESTIMATEGRADIENT( $\phi, \theta, f, h$ )
2:    $\nabla \phi := 0$ 
3:   for  $N$  do
4:      $\rho, \tau := \text{NORMAL}(\sigma_\rho), \text{NORMAL}(\sigma_\tau)$ 
5:      $s := (h(\rho, \phi) - f(\rho - \tau))^2$ 
6:      $\nabla \phi += \text{GRAD}(s, \phi)$ 
7:   end for
8:   return  $\nabla \phi / N$ 
9: end procedure

```

solve the rendering equation [Veach 1998]. We hence write Eq. 6 as

$$\frac{\partial}{\partial \phi} l = \int_{\Theta} \int_{\Theta} 2\lambda(\rho, \theta) \frac{\partial h(\rho, \phi)}{\partial \phi} h(\rho, \phi) d\tau - \int_{\Theta} 2\lambda(\rho, \theta) \frac{\partial h(\rho, \phi)}{\partial \phi} \kappa(\tau) f(\rho - \tau) d\tau d\rho, \quad (7)$$

where we use the fact that integrating an expression that is independent of the integration variable (here τ) reduces to multiplication by the volume of the integration domain, which we here assume to be normalized to unit volume, i.e., $\int_{\Theta} d\tau = 1$. Now the two inner integrals can be written as one, and factored as

$$\frac{\partial}{\partial \phi} l = \iint_{\Theta} 2\lambda(\rho, \theta) \frac{\partial h(\rho, \phi)}{\partial \phi} (h(\rho, \phi) - \kappa(\tau) f(\rho - \tau)) d\tau d\rho. \quad (8)$$

This integral spans the product space $\Theta \times \Theta$ and has the following unbiased estimator with linear complexity $\mathcal{O}(N)$:

$$\frac{\partial}{\partial \phi} l \approx \frac{1}{N} \sum_i \frac{2\lambda(\rho_i, \theta)}{p(\rho_i, \tau_i)} \frac{\partial h(\rho, \phi)}{\partial \phi} (h(\rho_i, \phi) - \kappa(\tau_i) f(\rho_i - \tau_i)), \quad (9)$$

$$= \frac{\partial}{\partial \phi} \frac{1}{N} \sum_i \frac{\lambda(\rho_i, \theta)}{p(\rho_i) p(\tau_i)} (h(\rho_i, \phi) - \kappa(\tau_i) f(\rho_i - \tau_i))^2. \quad (10)$$

It seems somewhat contrived to go through all the above reformulations to arrive from Eq. 4 at Eq. 9. Note, however, that differentiating *inside* the integral, enabled by Eq. 4, removes the non-linear function acting on the inner integral in Eq. 3 and hence enables us to formulate an *unbiased* estimator of the smoothed, localized loss in $\mathcal{O}(N)$. This re-formulation is only possible in special cases (here, for a second-order polynomial acting on the inner integral, see [Rainforth et al. 2018] Sec. 4) and would not be possible for other popular distance measures between h and f , e.g., the Kullback-Leibler (KL)-divergence or the Hinge- or Exponential-losses, which would introduce bias into the optimization due to non-linearities in their derivatives [Deng et al. 2022; Nicolet et al. 2023].

3.5 Sampling

For uniform random sampling, the MC estimator in Eq. 9 will exhibit substantial variance, leading to slower convergence and hence longer runtimes. Instead, we would like to sample in a way that maximizes a sample’s importance and therefore produces more meaningful gradients for the same sampling budget. Thanks to our

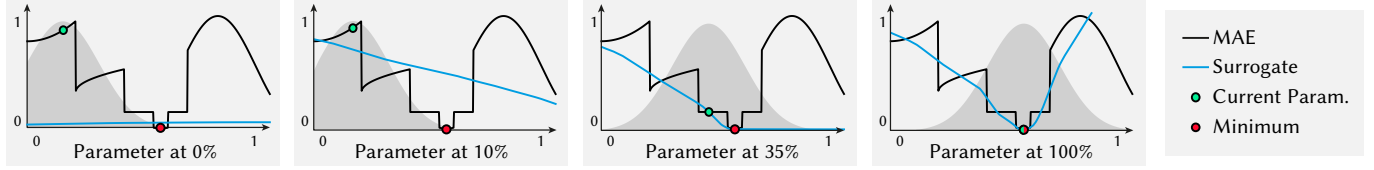


Fig. 4. A 1D-example with the function from Fig. 3a) and our neural surrogate (blue), which learns a local approximation of the loss (black, MAE) and provides gradients for the optimization parameter (green). The sampling distribution is displayed in grey, state is shown at 0%, 10%, 35% and 100% total iterations.

reformulation of the nested integral, it is evident that the integration domain now is $\Theta \times \Theta$, and that the magnitude of the gradient – the quantity we would like to estimate – is determined by three factors: the difference between the surrogate’s prediction and (smooth) objective f , and the locality terms λ and κ .

While we cannot trivially compute the probability density function (PDF) of the surrogate’s prediction error, our local surrogate formulation shows that we can reduce the variance by importance sampling [Veach 1998] for both locality terms. This again allows us to focus our surrogate on the regions of the parameter space that matter at the current optimization iteration while ignoring large amounts of space, which is especially helpful in higher dimensions. The parameter σ_o of the locality λ determines how far the current solution’s sampling radius is spread out, while σ_i determines the amount of smoothing, and is generally set to 15% of σ_o (for details, please see Suppl. Sec. 1.1). We display the resulting gradient estimator in Alg. 2.

3.6 Summary

In combination, the above elaborations allow us to optimize the objective function $f(\theta)$ through our surrogate’s *surrogate gradients* $\partial h/\partial \theta$. We emphasize that, in contrast to prior work [Grabocka et al. 2019; Hu et al. 2022a; Patel et al. 2020], our surrogate is learned self-supervised, without any ground truth supervision in the form of pre-computed gradients, and is optimized on-the-fly, alongside the parameter θ . This is made possible by a low number of samples which we achieve through our efficient estimators. As such, it allows the application of our method to systems where only a forward model is given. In the following sections, we will detail and evaluate some exemplary applications. Further, we provide a simple, illustrative 1D-example and visualize our learned surrogate loss over the course of the optimization in Fig. 4.

4 EVALUATION

Our evaluation compares different methods on a range of tasks (see Sec. 4.3 and Suppl. Sec. 2.2 for detailed task descriptions): we validate our design choices through ablations on lower-dimensional tasks in Sec. 4.3 and compare against established derivative-free optimizers on higher-dimensional, real-world tasks in Sec. 4.5. The reason for this is twofold: first, in the higher-dimensional regime, the task complexity makes it non-evident to see which of the ablated attributes lead to the method failing, and second, the derivative-free algorithms could solve some of the lower-dimensional tasks by simply brute-forcing the solution (which is a valid way of solving the problem, but besides the scope of interest here).

As our objective f , we use the mean-squared error (MSE) between the current rendered state and the target, if not otherwise specified. For details on our proxy’s architecture and hyperparameters, please see Suppl. Sec. 1.

4.1 Methods

We compare our approach to several ablations and variants, out of which some correspond to existing published methods. All methods operate in *image space* only and do not have access to any ground truth supervision or parameters. We structure the space of methods by the type of i) smoothing, ii) surrogate, and iii) sampling. Our full method, **Ours**, implements Alg. 2: it smooths the loss via convolution with a Gaussian (Eq. 1), uses a neural proxy and draws samples by importance-sampling the locality terms. We compare our full approach to the following methods and ablations:

NoSmooth, where we ablate the smoothing convolution (Eq. 1) and directly sample the non-smooth loss.

NoNN, where we replace the NN in the surrogate by a quadratic potential function of the form $(x, 1)^T M (x, 1)$, where, for an n -dimensional problem, M is a symmetric matrix in $\mathbb{R}^{n+1 \times n+1}$.

NoLocal, where we ablate the locality by drawing uniform random samples from the domain.

FD, our implementation of finite differences, with an optimally chosen $\pm \epsilon$ in each dimension.

FR22, which re-implements the approach presented by Fischer and Ritschel [2022b], who derive gradients by stochastically perturbing the optimization parameters θ at every iteration and weighting the resulting loss values by a gradient-of-Gaussian kernel, effectively creating a linear gradient estimate akin to a stochastic multi-sample version of Spall [1992].

4.2 Protocol

The results we report are the median values over an ensemble of 10 independent runs of random instances of each task. To ensure fairness, all methods are run in their best configuration. For each run, the parameter initialization and ground truth (where possible) are randomly re-sampled and the surrogate, optimizer and all other stateful components are re-initialized from scratch.

4.3 Tasks

We validate our method on two sets of tasks: the first set consists of lower-dimensional tasks from rendering, animation, modelling and physics, all of which are not trivially amenable to gradient-based optimization due to (partially) discrete parameter spaces, discontinuous integrals or non-differentiable frameworks, and serves the purpose of evaluating our approach’s design decisions. We provide

Table 2. An overview of our method and its ablations and competitors. To the right, we show the competitors’ relative error ratio at the iteration where our method achieves 95 % error reduction - i.e, how much others are behind.

Method	Smooth.	Surr. h	Sampler	Rend.	Model.	Anim.
NoSmooth	None	NN	Gauss	1.2 ×	3.9 ×	1.5 ×
NoNN	Gauss	Quad.	Gauss	8.9 ×	792.4 ×	16.3 ×
NoLocal	Gauss	NN	Uniform	12.3 ×	613.4 ×	22.4 ×
FD	None	Linear	Box	24.5 ×	654.3 ×	10.2 ×
FR22	Gauss	Linear	Import.	11.0 ×	323.6 ×	3.3 ×
Ours	Gauss	NN	Gauss	1.0 ×	1.0 ×	1.0 ×

a short description of each task in the following section and refer the reader to Suppl. Sec. 2.2 for more details on task setup and to Fig. 16 for task-specific visualizations.

Additionally, we evaluate how well our method scales to more realistic, higher-dimensional inverse optimization problems on a second set of tasks in Sec. 4.5.

4.3.1 Differentiable Rendering. Discontinuities in rendering arise from the visibility function that appears inside the integral, in which case the gradient of the integral cannot be computed as the integral of the gradient. Typical solutions include re-parametrization or edge-sampling for path tracing [Li et al. 2018; Loubet et al. 2019] or replacing step functions with soft counterparts in rasterization [Liu et al. 2019; Petersen et al. 2022] and use framework-specific implementations.

CORNELL-BOX We optimize the light’s horizontal and vertical translation and the axial rotation of both boxes inside the Cornell box. The discontinuities arise from visibility changes at the silhouette edges of the moving boxes and light.

BRDF Here, we optimize the material properties (RGB reflectance and index of refraction (IOR)) of a material test-ball illuminated under environment illumination. Optimizing properties of ideal specular objects, such as their IOR, often is challenging even for modern differentiable path tracers [Jakob et al. 2022b]. Our method does not make any assumptions on the underlying function, so we can successfully optimize these cases, too.

MOSAIC In this task, we simultaneously optimize the vertical rotation of 320 cubes to match a reference. Again, the discontinuities arise for pixels at the silhouette edges that change their color discontinuously with the occluding cube’s rotation.

4.3.2 Procedural Modelling. Procedural modelling mainly uses nodes from two categories, *filtering* nodes (that are differentiable by construction) and *generator* nodes, that operate on discrete parameters, such as a brick texture generator. Node relations often are highly non-linear due to complex material graphs and their interplay with other pipeline parameters. Moreover, the connections inside the nodegraph are a combinatorial problem with a highly discontinuous loss landscape. While previous research has made great progress in this field [Guerrero et al. 2022; Hu et al. 2022a,b; Li et al. 2023; Shi et al. 2020], it still often either involves lengthy, framework-specific pre-training, or relies on the existence of differentiable material libraries.

WICKER A procedural modelling scenario where we simultaneously optimize the parameters of a node graph that creates a woven wicker material. We optimize the number of horizontal and vertical stakes and the number of repetitions across the unit plane.

LED Given a target setting, we optimize each LED panel in a digital display to either be on or off. The display consists of 12 panels, each with 28 elements, leading to a 336-dim. binary problem.

NODE-GRAPH In this task, we directly optimize the connectivity of a material graph - a mixture of a combinatorial and procedural modelling problem. We encode all possible edges for a given set of nodes in a connection matrix and optimize the matrix entries. If an entry rounds to 1, the corresponding edge is inserted into the node graph, else removed. Our test graph has 8 nodes (several inputs and outputs each, 24 valid connections and matrix entries). Some graph edges constrain each other, e.g., when a shader node already is connected, a new connection will not result in an updated image, making this an even more inter-linked problem.

4.3.3 Animation. Accurate animation often relies on differential equations to solve the underlying physics equations which govern a character’s behaviour or movement. Oftentimes, the forward model of such an animation is inherently discontinuous (for instance, due to collisions) while at the same time, the underlying physics solver is not differentiable, as its output is the solution of an integral approximated by discrete sampling locations (the time steps). This is similar to the problem encountered in differentiable rendering: if the integrand (e.g., the time at which a force starts acting) is discontinuous, it is incorrect to simply differentiate the integral estimate to get a gradient estimate (see Suppl. Fig. 4).

ROCKET A physical simulation where we optimize the discrete event time at which a rocket’s engine must be turned off in order to reach a certain target point. We simultaneously optimize 10 rockets flying in parallel. As the forward model is solved with a finite number of time steps, a small change does not necessarily translate to a different outcome, leading to zero gradients almost everywhere.

GRAVITY This task runs a physics solver to infer the collision behaviour of three cubes that are dropped onto each other. If optimized correctly, the cubes will form a tower after being dropped. We optimize the two upper cubes’ initial translation and their coefficients of restitution, the “bounciness”, which we provide as the input to the solver.

4.4 Results

We display the results of all methods listed in Tab. 2 in Fig. 15, with one subfigure per task, and show a quantitative analysis in the right part of Tab. 2. We group the results into rendering (**CORNELL BOX**, **BRDF**, **MOSAIC**), modelling (**WICKER**, **NODE-GRAPH**, **LED**) and animation (**ROCKET**, **GRAVITY**), which correspond to the three rightmost columns in Tab. 2 and the rows in Fig. 15, respectively.

From the convergence plots in Fig. 15, it becomes evident that **NoLocal** works in select cases, but often struggles to find the correct solution, especially where the domain is higher-dimensional (e.g., **MOSAIC**), as a uniform random sampling of the parameter space introduces substantial variance in the gradient estimates. Similarly, **NoNN** is challenged in higher-dimensional cases and does not converge reliably, which we attribute to the reduced expressiveness of

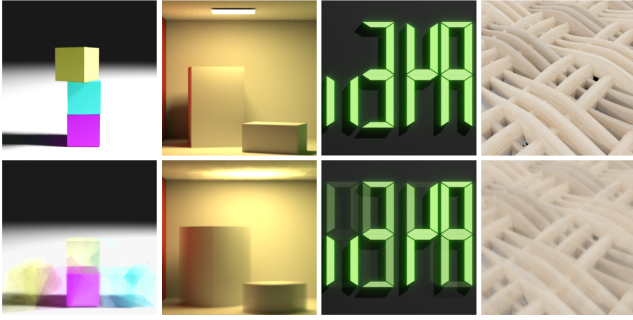


Fig. 5. Samples of the smooth objective (bottom row) on which we learn our surrogate: Perturbing the rigid scene parameters (top row) smooths discontinuities, e.g., the binary on/off for the **LED** task (an inset is shown).

the quadratic potential. However, this shows that for simple tasks (e.g., **CORNELL-BOX**), the proxy does not need to be overly complicated. Finite Differences (**FD**) works well and makes steady progress towards the target, but does not scale well to higher dimensions, as an n -dimensional problem requires $2n$ function evaluations for a single gradient step (see the wall-time plots in Fig. 15 and Tab. 1). **FR22** works reliably on all tasks, but often converges slower than our method. Surprisingly, we find that ablating the inner smoothing operation in **NoSmooth** only slightly impedes performance (ca. 2x), which we partly attribute to the implicit smoothing introduced by the surrogate fit. In almost all cases, **Ours** works best and faithfully recovers the true parameters. The overhead of our method compared to its competitors is small: for smoothing, it suffices to slightly perturb the current state, i.e., no additional evaluation of f is required. The NN query is very efficient as it can be parallelized on the GPU, and the surrogates are relatively shallow (for implementation details see Suppl. Sec. 1), providing **Ours** with the best quality-speed relation, as is evident from the right bottom subfigure in Fig. 15, where we show the (normalized and re-sampled) mean performance of all methods.

4.5 Higher Dimensions

We here evaluate our method on higher-dimensional problems from the inverse rendering literature and compare our approach against the established derivative-free optimizers genetic algorithms (**GA**) [Holland 1973], simulated annealing (**SA**) [Kirkpatrick et al. 1983], simultaneous perturbation stochastic approximation (**SPSA**) [Spall 1992] and **CMA-ES** [Hansen 2016]. Due to the high dimensionality of these experiments, we found it necessary to increase the surrogate capacity and the gradient batchsize (for implementation details, please see Suppl. Sec. 1). All results we show are equal-sample comparisons, i.e., achieved after the same number of function evaluations, disregarding the fact that **CMA** requires significantly (multiple times) more runtime than all other approaches. To avoid clutter in the main manuscript, we show the outcome of our ablated methods on these tasks in Suppl. Fig. 2.

TEXTURE First, we optimize the 256×256 RGB pixels of a texture in Fig. 6, a relatively simple task with a smooth cost landscape and no correlation between the optimization variables. Our surrogate gradients lead to a successful optimization outcome, while

the derivative-free optimizers **GA** and **SA** fail to converge due to the high problem dimensionality. **CMA** cannot be run on our 64GB RAM machine because of the quadratic memory requirements of the covariance matrix. Both **SPSA** and **FR22** make progress towards the target, but require more time to converge.

MLP To increase the correlation between the optimization variables from the previous task, we repeat a similar experiment in Fig. 7, where we use our method to optimize the weights of a multi-layered perceptron (MLP) such that it overfits single digits from the MNIST [LeCun 1998] dataset, i.e., learns a mapping from continuous 2D coordinates in $(0,1)$ to a monochrome color value at the corresponding pixel location. The results are similar: our method has already converged, while **SPSA** and **CMA** make progress but require more function evaluations, and both **GA** and **SA** do not converge at all. Interestingly, **FR22** does not converge either. This is in line with recent findings that show that perturbation-based methods do not perform well on emulating backpropagation in neural networks [Belouze 2022; Chandra 2021; Nesterov and Spokoyny 2017].

MESH Next, we optimize the 3D position of 2,562 vertices of a triangle mesh, as in Nicolet et al. [2021], to match a reference (Fig. 8). This problem is already much harder, as the vertices are interlinked and the loss landscape exhibits discontinuities due to the rasterization process. On this task, **GA** and **SPSA** fail to converge to the correct result, while **SA** does not move from the initial configuration. In contrast, **CMA**, **FR22** and **Ours** find the correct solution, with **FR22** and **Ours** achieving the lowest final optimization errors (0.0018 and 0.0013, respectively). For completeness, we also show the differentiable rendering solution proposed by [Nicolet et al. 2021].

CAUSTIC In caustic optimization, a classic task from inverse rendering [Kiser et al. 2013; Papas et al. 2011; Schwartzburg et al. 2014], the goal is to optimize an initial height-field such that it refracts incoming light into a caustic that resembles a provided reference image. While previous systems have gone to great effort to accurately capture the intricate behaviour of the refracted light, we use a simple rasterization-based renderer inspired by [Wyman and Davis 2006] (for details see Suppl. Sec. 2.2). Our heightfield is parameterized by a cubic B-Spline with resolution 1,024. This example is interesting as the optimization variables have a highly non-local influence on the observed image pixels. We show the resulting optimization outcomes in Fig. 9 and observe that all traditional gradient-free optimizers fail to correctly recover the target image. Again, **SPSA** and **FR22** achieve a caustic that roughly resembles the reference, while our method achieves a plausible outcome.

SPLINE GENERATION Finally, we use our method to train a *generative model* on a *non-differentiable* task. Here, we use our surrogate gradients to train a VAE [Kingma and Welling 2013] that encodes digits from the MNIST [LeCun 1998] dataset and outputs the support points of a spline curve, which are then rendered with a non-differentiable spline renderer. As in all tasks, we operate in *image space* only, so we cannot simply backpropagate through the spline renderer, but must query our surrogate for gradients.

This again is a very high-dimensional, non-local and interlinked problem, as all optimization variables (the NN weights) directly influence the spline’s final support points. For details on the training and model architecture, please see Suppl. Sec. 2.2. In Fig. 10,

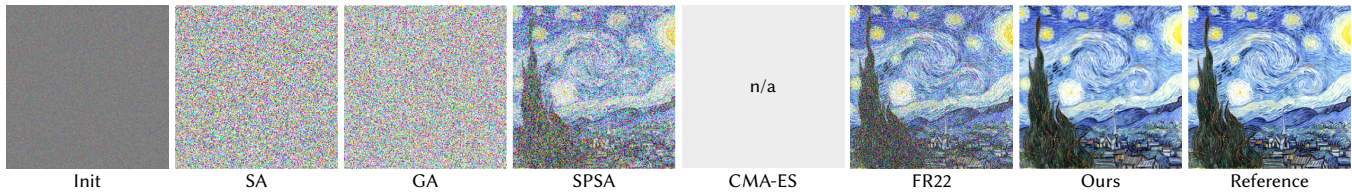


Fig. 6. We show an equal-sample comparison (i.e., the same budget of function evaluations) for the task of optimizing a $256 \times 256 \times 3$ texture. CMA-ES cannot be run on this example due to its quadratic memory complexity causing out-of-memory errors on our 64 GB RAM machine.

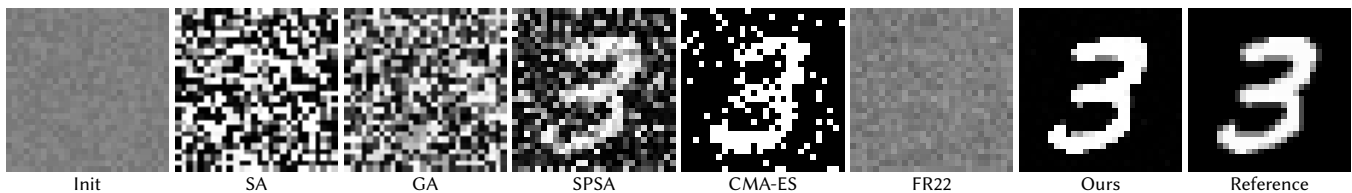


Fig. 7. We show an equal-sample comparison for the task of optimizing the 35,152 weights of a MLP such that it encodes digits from MNIST [LeCun 1998].

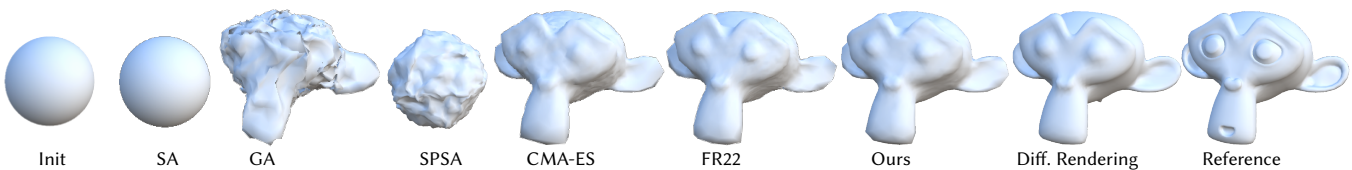


Fig. 8. We show an equal-sample comparison for the task of optimizing the 3D positions of a tessellated sphere with 2,562 vertices to match a rendered reference shape. “Diff. Rendering” uses the analytical gradients from Nicolet et al. [2021].

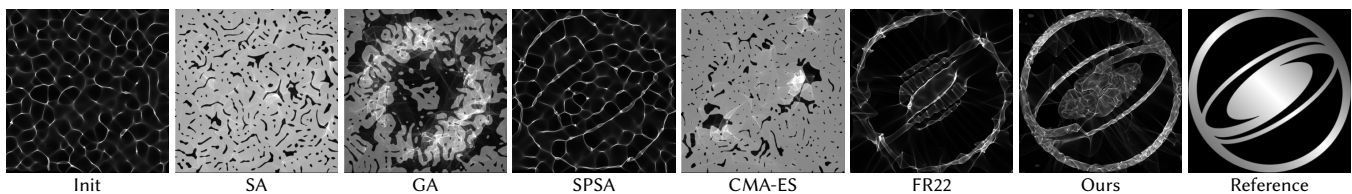


Fig. 9. We show an equal-sample comparison for the task of optimizing a 1,024-dim. heightfield such that the resulting caustic resembles the reference image.

we sample the latent space of the model after training. We render the generated spline in different styles, which can easily be applied in post-processing due to the control-point formulation. As is evident from the figure, our method is the only approach that achieves an output that resembles actual digits across all numbers, with FR22 achieving satisfactory results on simple cases (1, 3, 5, 7), and the other derivative-free optimizers failing completely. To our knowledge, this is the first generative model that is trained on a non-differentiable task, which again highlights the generality of our proposed approach, ZeroGrads, and gives rise to an exciting avenue of future research.

4.6 Gradient Variance Analysis

While our method works well in all the previous tasks, its benefits are most pronounced when the loss landscape exhibits stochasticity or noise, e.g., in the **MLP** and **SPLINES** tasks. We hypothesize that

this can be explained by the centerpiece of our approach, the *neural proxy*: in contrast to FR22 and SPSA, ZeroGrads uses a neural network as proxy function, whose state acts as hysteresis and endows our method with a certain inertia, limiting the estimated loss landscape’s spatiotemporal change by the network’s adaptability. This behaviour is further reinforced by the spectral bias of neural networks [Rahaman et al. 2019; Tancik et al. 2020], which has been shown to encourage the learning of low-frequency, Lipschitz-continuous functions over those characterized by rapid changes.

FR22 and SPSA, in contrast, re-build a (linear) gradient estimate during every iteration of the optimization, effectively ignoring information about the loss landscape from previous iterations. As this gradient estimate is a stochastic approximation, it will exhibit noise and variance, which highlights the main difference between the discussed (gradient-based) approaches: while SPSA and FR22 estimate the *parameter gradient* ∂_{θ} (subject to variance), ZeroGrads estimates the *surrogate gradient* ∂_{ϕ} , but *analytically* computes the

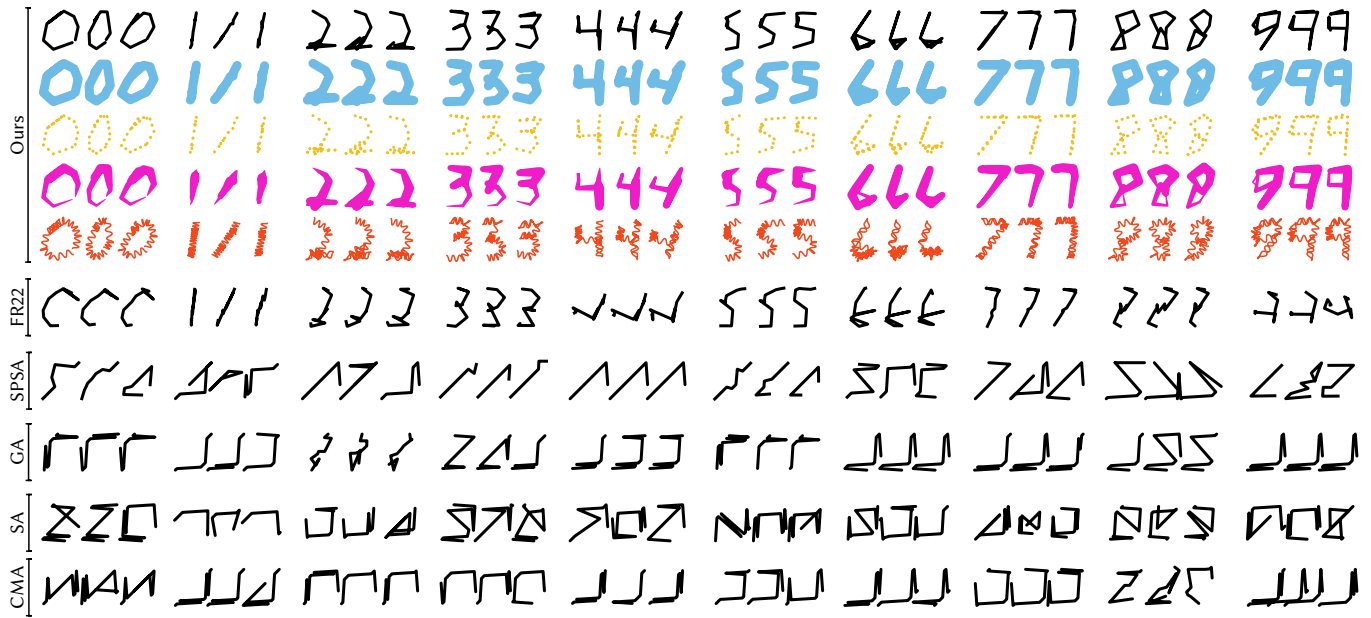


Fig. 10. We sample the latent space of our trained variational autoencoder (VAE) and show a variety of style transformations (rows), enabled by the spline formulation, on three digits per MNIST class. The first row displays the output of the spline renderer on which the surrogate operates.

parameter gradient ∂_θ . This allows us to move the higher-variance estimate into the neural network’s parameter update, where the estimate’s noise is smoothed by the aforementioned hysteresis.

To analyze this behaviour, we plot the variance of the gradient-magnitude over the course of the optimization in Fig. 11 for all three gradient-based optimizers *SPSA*, *FR22* and *Ours*. The vastly different scales on the y-axes of each subplot confirm our hypothesis: the variance in the gradient-magnitude of our method is consistently orders of magnitude lower than that of the other approaches. While this does not allow reasoning about the *correctness* of the derived gradients, it explains why our approach outperforms the competitors in the provided examples.

4.7 Comparison to specific solutions

There exist many specialized solutions that enable gradient computation in graphics, and a full study of *all* is beyond the scope of this work. We compare qualitatively to two of these methods, rendering (Fig. 12) and procedural modelling (Fig. 13), where the common theme is that our neural surrogates are capable of optimizing their specific problems as well, and sometimes even go beyond. In Fig. 12, top row, we show that we can optimize a material’s IOR, a feature for which backpropagation through detached sampling has not yet been implemented in Mitsuba. As our method only needs a forward-model, we can simply combine Mitsuba’s forward path tracer with our surrogate gradients and thus are able to optimize the IOR as well. In Fig. 13, we optimize a node graph towards the target patterns, using a mixture of VGG and MSE loss, which nicely shows our surrogate’s flexibility w.r.t. to the objective f . Moreover, our

¹We exclude finite differences from this comparison due to its intractable per-iteration cost in higher dimensions.

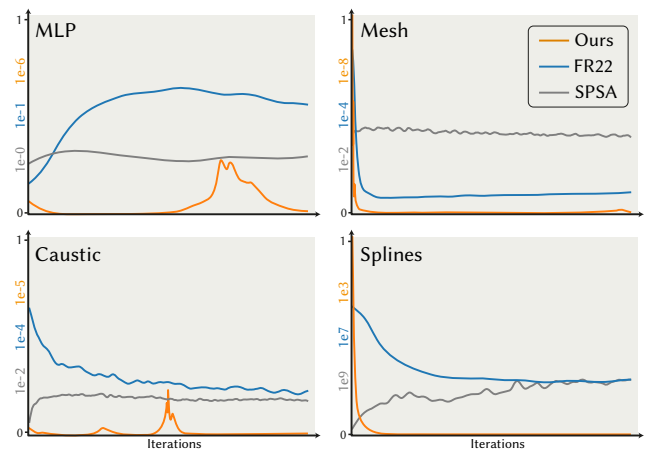


Fig. 11. We plot the variance (smoothed for ease of visualization) of the gradient magnitude over the course of the optimization. Note that the scales are vastly different, as denoted on the left axis. Our method consistently produces gradients with lower-variance magnitude, which we attribute to the neural proxy’s state and smoothness, resulting in less gradient noise.

method also works in extreme parameter ranges, as is evident from the bottom row in Fig. 13, where the pre-trained proxy from Hu et al. [2022a] breaks due to the parameter value being out of the range it encountered during training. In summary, although our method might sometimes come at the expense of higher compute or variance (e.g., compared to Mitsuba in Fig. 12, see the convergence plots to the right), the strength of our approach lies in its generality, i.e., in that it can be applied to arbitrary forward graphic models, and that it successfully optimizes high-dimensional, interlinked problems.

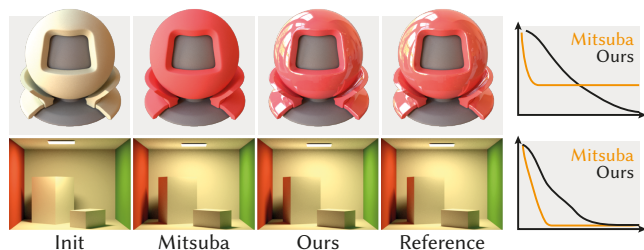


Fig. 12. Comparison with Mitsuba 3 [Jakob et al. 2022b] on the **BRDF** and **CORNELL-BOX** tasks, top and bottom row, respectively. Note that the incorrect IOR in the top row is due to Mitsuba not yet implementing this feature instead of failing during optimization (see Sec. 4.7).

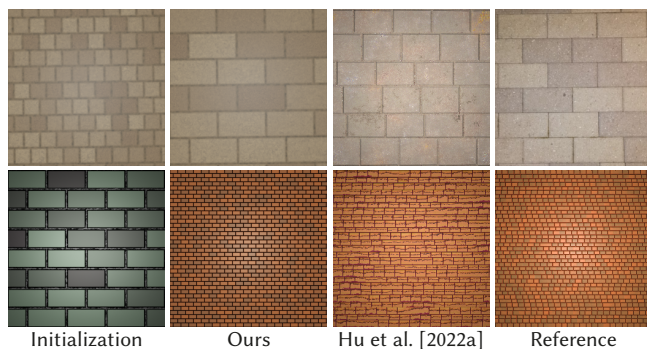


Fig. 13. Comparison between Ours and Hu et al. [2022a] (result and reference taken from their publication). In the lower row, their pre-trained brick generator fails, as the parameter lies outside the training domain.

4.8 Limitations and Failure Cases

Our method inherits the limitations of gradient descent, namely that it can get stuck in local minima (although we do our best to avoid this via the smoothing convolution), move slowly in regions of shallow slope (see the experiments on the Rosenbrock function in Suppl. Fig. 1) and that it introduces additional hyperparameters (Suppl. Sec. 1.1). Additionally, our method “wastes” samples during an initial warm-up phase, in which the (initially random) network weights first adapt to the loss landscape. Moreover, while our derived gradients have lower variance than competing approaches (Fig. 11), they have higher variance than analytical gradients and therefore typically under-perform relative to problem-specific methods, where they are available (see the convergence plots in Fig. 12). Finally, on lower-dimensional discrete problems, it can potentially be faster to simply brute-force the solution by trying all possible combinations, akin to what genetic algorithms would do with a high-enough sample budget. However, this quickly becomes infeasible as dimensionality increases.

In addition, we show a failure case in Fig. 14. The task is inspired by PSDR-Room [Nguyen et al. 2012; Yan et al. 2023] and the optimizer is asked to replicate a scene layout and materials from a single photograph. For each piece of furniture or shrubbery, the optimizer can make a discrete choice from 10 objects (left column in Fig. 14) and additionally adapt their continuous 3D position in

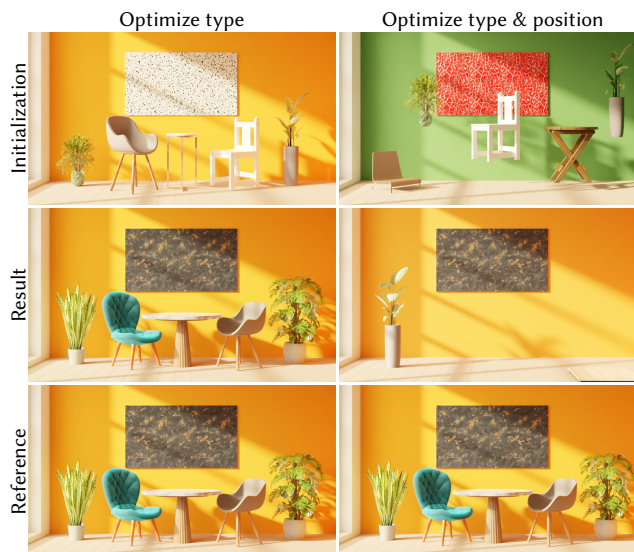


Fig. 14. A limitation of our method: when the loss landscape is too complex (right column: mixture of plateaus and discrete spaces), the proxy cannot encode it accurately and the optimization stalls in a local minimum.

the scene and the wall’s color (right column in Fig. 14). We optimize MSE in the single-stage, single-resolution setting. While successful in the type-only setting, ZeroGrads fails to correctly optimize both type and position in the right column of Fig. 14. We assume this is because the optimizer must cycle through a number of objects before encountering the correct one, while simultaneously working in discrete and continuous space, and moreover dealing with plateaus in image-space which stem from the objects not overlapping their reference counterparts. Not even the smoothing operation can make this task easier, as the optimizer has the opportunity to reduce the image error by simply pushing the objects out-of-frame (as is happening here) and then falls into a local minimum from which it cannot recover. We conclude that more research is needed in this direction, e.g., through self-adapting proxy configurations or advanced hybrid approaches.

5 CONCLUSION

We have proposed ZeroGrads, a method for practical computation of surrogate gradients in non-differentiable black-box pipelines, as are found across many graphics domains, ranging from rendering over modelling to animation. Our key ideas are the smoothing of the loss landscape, a local approximation thereof by a NN, and a low-variance estimator based on sparse, local sampling. We have favourably compared to several ablations and published alternatives and shown results for a wide variety of tasks. Additionally, our neural surrogate allows us to transform the noisy gradient estimate into an update on the network’s parameters, where the noise is smoothed by the network’s hysteresis. We therefore can show that our surrogate gradients scale to high dimensionality, where traditional gradient-free optimization algorithms often do not converge.

In future work, we plan to further explore the interplay of the inner surrogate loss and the outer optimizer and to find ways to automatically determine the required surrogate network's complexity. Moreover, it would be interesting to leverage the fact that our surrogate provides a continuous model of the cost landscape, for instance by lookahead-training or approximate second-order methods.

Most of the things that enable our approach are known in the optimization community that routinely uses proxies and surrogates. Yet, these ideas are rarely used in graphics, where specific solutions were developed and rarely compared against what the optimization literature offers. Our work combines graphic-specific features (e.g., MC-estimating the gradient, sampling the objective through simply rendering) and graphics-inspired improvements (such as variance reduction through importance sampling) to match requirements of graphics with general optimization.

ACKNOWLEDGMENTS

This work was supported by Meta Reality Labs, Grant Nr. 5034015. Michael is further supported by a bursary from the Rabin Ezra scholarship trust.

REFERENCES

- Navid Ansari, Hans-Peter Seidel, Nima Vahidi Ferdowsi, and Vahid Babaei. 2022. Autoinverse: Uncertainty aware inversion of neural networks. *Advances in Neural Information Processing Systems* 35 (2022), 8675–8686.
- Sai Bangaru, Lifan Wu, Tzu-Mao Li, Jacob Munkberg, Gilbert Bernstein, Jonathan Ragan-Kelley, Fredo Durand, Aaron Lefohn, and Yong He. 2023. SLANG.D: Fast, Modular and Differentiable Shader Programming. *ACM Transactions on Graphics (SIGGRAPH Asia)* 42, 6 (December 2023), 1–28. <https://doi.org/10.1145/3618353>
- Sai Praveen Bangaru, Michaël Gharbi, Tzu-Mao Li, Fujun Luan, Kalyan Sunkavalli, Miloš Hašan, Sai Bi, Zexiang Xu, Gilbert Bernstein, and Frédo Durand. 2022. Differentiable Rendering of Neural SDFs through Reparameterization. *arXiv preprint arXiv:2206.05344* (2022).
- Sai Praveen Bangaru, Jesse Michel, Kevin Mu, Gilbert Bernstein, Tzu-Mao Li, and Jonathan Ragan-Kelley. 2021. Systematically differentiating parametric discontinuities. *ACM Trans. Graph.* 40, 4 (2021), 1–18.
- Russell R Barton. 1994. Metamodeling: a state of the art review. In *Proceedings of Winter Simulation Conference*. IEEE, 237–244.
- Gabriel Belouze. 2022. Optimization without Backpropagation. *arXiv preprint arXiv:2209.06302* (2022).
- Quentin Berthet, Mathieu Blondel, Olivier Teboul, Marco Cuturi, Jean-Philippe Vert, and Francis Bach. 2020. Learning with differentiable perturbed optimizers. *Advances in neural information processing systems* 33 (2020), 9508–9519.
- George EP Box and Norman R Draper. 1987. *Empirical model-building and response surfaces*. John Wiley & Sons.
- James Bradbury, Roy Frostig, Peter Hawkins, Matthew James Johnson, Chris Leary, Dougal Maclaurin, George Necula, Adam Paszke, Jake VanderPlas, Skye Wanderman-Milne, and Qiao Zhang. 2018. JAX: composable transformations of Python+NumPy programs. <http://github.com/google/jax>
- Kartik Chandra. 2021. An Unexpected Challenge in Using Forward-Mode Automatic Differentiation for Low-Memory Deep Learning. *Undergrad Theses* (2021).
- Kartik Chandra, Tzu-Mao Li, Joshua Tenenbaum, and Jonathan Ragan-Kelley. 2022. Designing Perceptual Puzzles by Differentiating Probabilistic Programs. In *Proc. SIGGRAPH*. Article 21, 9 pages.
- Michael B Chang, Tomer Ullman, Antonio Torralba, and Joshua B Tenenbaum. 2016. A compositional object-based approach to learning physical dynamics. *arXiv preprint arXiv:1612.00341* (2016).
- Swarat Chaudhuri and Armando Solar-Lezama. 2010. Smooth interpretation. *ACM Sigplan Notices* 45, 6 (2010), 279–291.
- Per Christensen, Julian Fong, Jonathan Shade, Wayne Wooten, Brenden Schubert, Andrew Kensler, Stephen Friedman, Charlie Kilpatrick, Cliff Ramshaw, Marc Bannister, et al. 2018. Renderman: An advanced path-tracing architecture for movie rendering. *ACM Trans. Graph.* 37, 3 (2018), 1–21.
- Jia Deng, Wei Dong, Richard Socher, Li-Jia Li, Kai Li, and Li Fei-Fei. 2009. Imagenet: A large-scale hierarchical image database. In *2009 IEEE conference on computer vision and pattern recognition*. Ieee, 248–255.
- Xi Deng, Fujun Luan, Bruce Walter, Kavita Bala, and Steve Marschner. 2022. Reconstructing translucent objects using differentiable rendering. In *ACM SIGGRAPH 2022 Conference Proceedings*. 1–10.
- John C Duchi, Peter L Bartlett, and Martin J Wainwright. 2012. Randomized smoothing for stochastic optimization. *SIAM Journal on Optimization* 22, 2 (2012), 674–701.
- Hadi Esmaeilzadeh, Adrian Sampson, Luis Ceze, and Doug Burger. 2012. Neural acceleration for general-purpose approximate programs. In *2012 45th Annual IEEE/ACM International Symposium on Microarchitecture*. IEEE, 449–460.
- Michael Fischer, Konstantin Kobs, and Andreas Hotho. 2020. NICER: Aesthetic image enhancement with humans in the loop. *arXiv preprint arXiv:2012.01778* (2020).
- Michael Fischer and Tobias Ritschel. 2022a. Metappearance: Meta-Learning for Visual Appearance Reproduction. *ACM Trans. Graph.* 41, 6 (2022), 1–13.
- Michael Fischer and Tobias Ritschel. 2022b. Plateau-free Differentiable Path Tracing. *arXiv preprint arXiv:2211.17263* (2022).
- Alexander IJ Forrester and Andy J Keane. 2009. Recent advances in surrogate-based optimization. *Progress in aerospace sciences* 45, 1–3 (2009), 50–79.
- Marc-André Gardner, Yannick Hold-Geoffroy, Kalyan Sunkavalli, Christian Gagné, and Jean-François Lalonde. 2019. Deep parametric indoor lighting estimation. In *Proc. ICCV*. 7175–83.
- Josif Grabocka, Randolph Scholz, and Lars Schmidt-Thieme. 2019. Learning surrogate losses. *arXiv preprint arXiv:1905.10108* (2019).
- Radek Grzeszczuk, Demetri Terzopoulos, and Geoffrey Hinton. 1998. Neuroanimator: Fast neural network emulation and control of physics-based models. In *Proc. SIGGRAPH*. 9–20.
- Paul Guerrero, Miloš Hašan, Kalyan Sunkavalli, Radomír Měch, Tamy Boubekeur, and Niloy J Mitra. 2022. Matformer: A generative model for procedural materials. *arXiv preprint arXiv:2207.01044* (2022).
- H-M Gutmann. 2001. A radial basis function method for global optimization. *J global optimization* 19, 3 (2001), 201–227.
- John K Haas. 2014. A history of the unity game engine. *Diss. WORCESTER POLYTECHNIC INSTITUTE* 483 (2014), 484.
- Marc Habermann, Lingjie Liu, Weipeng Xu, Michael Zollhoefer, Gerard Pons-Moll, and Christian Theobalt. 2021. Real-time deep dynamic characters. *ACM Trans. Graph.* 40, 4 (2021), 1–16.
- Nikolaus Hansen. 2016. The CMA evolution strategy: A tutorial. *arXiv preprint arXiv:1604.00772* (2016).
- Philipp Holl, Vladen Koltun, and Nils Thuerey. 2020. Learning to control pdes with differentiable physics. *arXiv preprint arXiv:2001.07457* (2020).
- John H Holland. 1973. Genetic algorithms and the optimal allocation of trials. *SIAM journal on computing* 2, 2 (1973), 88–105.
- Yuanming Hu, Luke Anderson, Tzu-Mao Li, Qi Sun, Nathan Carr, Jonathan Ragan-Kelley, and Frédo Durand. 2019. DiffTaichi: Differentiable programming for physical simulation. *arXiv preprint arXiv:1910.00935* (2019).
- Yiwei Hu, Paul Guerrero, Milos Hasan, Holly Rushmeier, and Valentin Deschaintre. 2022a. Node Graph Optimization Using Differentiable Proxies. In *Proc. SIGGRAPH*. 1–9.
- Yiwei Hu, Chengan He, Valentin Deschaintre, Julie Dorsey, and Holly Rushmeier. 2022b. An inverse procedural modeling pipeline for svbrdf maps. *ACM Trans. Graph.* 41, 2 (2022), 1–17.
- Wenzel Jakob, Sébastien Speierer, Nicolas Roussel, Merlin Nimier-David, Delio Vicini, Tizian Zeltner, Baptiste Nicolet, Miguel Crespo, Vincent Leroy, and Ziyi Zhang. 2022b. Mitsuba 3 Renderer, 2022.
- Wenzel Jakob, Sébastien Speierer, Nicolas Roussel, and Delio Vicini. 2022a. Dr. jit: A just-in-time compiler for differentiable rendering. *ACM Transactions on Graphics (TOG)* 41, 4 (2022), 1–19.
- Kevin G Jamieson, Robert Nowak, and Ben Recht. 2012. Query complexity of derivative-free optimization. *Advances in Neural Information Processing Systems* 25 (2012).
- Donald R Jones, Matthias Schonlau, and William J Welch. 1998. Efficient global optimization of expensive black-box functions. *J Global optimization* 13, 4 (1998), 455–92.
- Herman Kahn. 1950. Random sampling (Monte Carlo) techniques in neutron attenuation problems. I. *Nucleonics (US) Ceased publication* 6. See also NSA 3-990 (1950).
- James T Kajiya. 1986. The rendering equation. In *Proceedings of the 13th annual conference on Computer graphics and interactive techniques*. 143–150.
- Hiroharu Kato, Yoshitaka Ushiku, and Tatsuya Harada. 2018. Neural 3D mesh renderer. In *Proc. CVPR*. 3907–16.
- Diederik P Kingma and Max Welling. 2013. Auto-encoding variational bayes. *arXiv preprint arXiv:1312.6114* (2013).
- Scott Kirkpatrick, C Daniel Gelatt Jr, and Mario P Vecchi. 1983. Optimization by simulated annealing. *science* 220, 4598 (1983), 671–680.
- Thomas Kiser, Michael Eigensatz, Minh Man Nguyen, Philippe Bompas, and Mark Pauly. 2013. Architectural caustics—controlling light with geometry. In *Advances in architectural geometry 2012*. Springer, 91–106.
- Averill M Law, W David Kelton, and W David Kelton. 2007. *Simulation modeling and analysis*. Vol. 3. Mcgraw-hill New York.
- Quentin Le Lidec, Ivan Laptev, Cordelia Schmid, and Justin Carpentier. 2021. Differentiable rendering with perturbed optimizers. *Advances in Neural Information Processing Systems* 34 (2021), 20398–20409.

- Yann LeCun. 1998. The MNIST database of handwritten digits. <http://yann.lecun.com/exdb/mnist/> (1998).
- Wonyeol Lee, Hangyeol Yu, and Hongseok Yang. 2018. Reparameterization gradient for non-differentiable models. *Proc. NeurIPS* 31 (2018).
- Beichen Li, Liang Shi, and Wojciech Matusik. 2023. End-to-End Procedural Material Capture with Proxy-Free Mixed-Integer Optimization. *ACM Transactions on Graphics (TOG)* 42, 4 (2023), 1–15.
- Tzu-Mao Li, Miika Aittala, Frédo Durand, and Jaakko Lehtinen. 2018. Differentiable Monte Carlo ray tracing through edge sampling. *ACM Trans. Graph.* 37, 6 (2018), 1–11.
- Tzu-Mao Li, Michal Lukáč, Michaël Gharbi, and Jonathan Ragan-Kelley. 2020. Differentiable vector graphics rasterization for editing and learning. *ACM Trans. Graph.* 39, 6 (2020), 1–15.
- Shichen Liu, Tianye Li, Weikai Chen, and Hao Li. 2019. Soft rasterizer: A differentiable renderer for image-based 3D reasoning. In *Proc. ICCV*. 7708–17.
- Matthew M Loper and Michael J Black. 2014. OpenDR: An approximate differentiable renderer. In *Proc. ECCV*. Springer, 154–169.
- Guillaume Loubet, Nicolas Holzschuch, and Wenzel Jakob. 2019. Reparameterizing discontinuous integrands for differentiable rendering. *ACM Trans. Graph.* 38, 6 (2019), 1–14.
- Joe Marks, Brad Andalman, Paul A Beardsley, William Freeman, Sarah Gibson, Jessica Hodgins, Thomas Kang, Brian Mirtich, Hanspeter Pfister, Wheeler Ruml, et al. 1997. Design galleries: A general approach to setting parameters for computer graphics and animation. In *Proc. SIGGRAPH*. 389–400.
- Luke Metz, C Daniel Freeman, Samuel S Schoenholz, and Tal Kachman. 2021. Gradients are not all you need. *arXiv preprint arXiv:2111.05803* (2021).
- Shakir Mohamed, Mihaela Rosca, Michael Figurnov, and Andriy Mnih. 2020. Monte Carlo Gradient Estimation in Machine Learning. *J. Mach. Learn. Res.* 21 (2020).
- Louis Montaut, Quentin Le Lidec, Antoine Bambade, Vladimir Petrik, Josef Sivic, and Justin Carpentier. 2023. Differentiable collision detection: a randomized smoothing approach. In *2023 IEEE International Conference on Robotics and Automation (ICRA)*. IEEE, 3240–3246.
- Damian Mrowca, Chengxu Zhuang, Elias Wang, Nick Haber, Li F Fei-Fei, Josh Tenenbaum, and Daniel L Yamins. 2018. Flexible neural representation for physics prediction. *Proc. NeurIPS* 31 (2018).
- Andreas Munk, Adam Ścibior, Atılım Güneş Baydin, Andrew Stewart, Goran Fernlund, Anoush Poursartip, and Frank Wood. 2019. Deep probabilistic surrogate networks for universal simulator approximation. *arXiv preprint arXiv:1910.11950* (2019).
- Oliver Nalbach, Elena Arabadzhiyska, Dushyant Mehta, H-P Seidel, and Tobias Ritschel. 2017. Deep shading: convolutional neural networks for screen space shading. In *Comp. Graph. Forum*, Vol. 36. 65–78.
- Jiří Navrátil, Alan King, Jesus Rios, Georgios Kollias, Ruben Torrado, and Andrés Codas. 2019. Accelerating physics-based simulations using end-to-end neural network proxies: An application in oil reservoir modeling. *Frontiers in big Data* 2 (2019), 33.
- Yurii Nesterov and Vladimir Spokoiny. 2017. Random gradient-free minimization of convex functions. *Foundations of Computational Mathematics* 17 (2017), 527–566.
- Chuong H Nguyen, Tobias Ritschel, Karol Myszkowski, Elmar Eisemann, and Hans-Peter Seidel. 2012. 3D material style transfer. In *Computer Graphics Forum*, Vol. 31. Wiley Online Library, 431–438.
- Baptiste Nicolet, Alec Jacobson, and Wenzel Jakob. 2021. Large Steps in Inverse Rendering of Geometry. *ACM Transactions on Graphics (Proceedings of SIGGRAPH Asia)* 40, 6 (Dec. 2021). <https://doi.org/10.1145/3478513.3480501>
- Baptiste Nicolet, Fabrice Rousselle, Jan Novak, Alexander Keller, Wenzel Jakob, and Thomas Müller. 2023. Recursive Control Variates for Inverse Rendering. *ACM Transactions on Graphics (TOG)* 42, 4 (2023), 1–13.
- Marios Papas, Wojciech Jarosz, Wenzel Jakob, Szymon Rusinkiewicz, Wojciech Matusik, and Tim Weyrich. 2011. Goal-based caustics. In *Computer Graphics Forum*, Vol. 30. Wiley Online Library, 503–511.
- Konstantinos E Parsopoulos and Michael N. Vrahatis. 2002. Recent approaches to global optimization problems through particle swarm optimization. *Natural computing* 1, 2 (2002), 235–306.
- Adam Paszke, Sam Gross, Soumith Chintala, Gregory Chanan, Edward Yang, Zachary DeVito, Zeming Lin, Alban Desmaison, Luca Antiga, and Adam Lerer. 2017. Automatic differentiation in pytorch. (2017).
- Yash Patel, Tomáš Hodaň, and Jiří Matas. 2020. Learning surrogates via deep embedding. In *Proc. ECCV*. Springer, 205–221.
- Felix Petersen, Bastian Goldluecke, Christian Borgelt, and Oliver Deussen. 2022. GenDR: A Generalized Differentiable Renderer. In *Proc. CVPR*. 4002–4011.
- Michael JD Powell. 1994. A direct search optimization method that models the objective and constraint functions by linear interpolation. In *Advances in optimization and numerical analysis*. Springer, 51–67.
- Nestor V Queipo, Raphael T Haftka, Wei Shyy, Tushar Goel, Rajkumar Vaidyanathan, and P Kevin Tucker. 2005. Surrogate-based analysis and optimization. *Progress in aerospace sciences* 41, 1 (2005), 1–28.
- Nasim Rahaman, Aristide Baratin, Devansh Arpit, Felix Draxler, Min Lin, Fred Hamprecht, Yoshua Bengio, and Aaron Courville. 2019. On the spectral bias of neural networks. In *International Conference on Machine Learning*. PMLR, 5301–5310.
- Gilles Rainer, Wenzel Jakob, Abhijeet Ghosh, and Tim Weyrich. 2019. Neural BTF compression and interpolation. In *Comp. Graph. Forum*, Vol. 38. 235–44.
- Tom Rainforth, Rob Cornish, Hongseok Yang, Andrew Warrington, and Frank Wood. 2018. On nesting Monte Carlo estimators. In *Proc. ICML*. PMLR, 4267–4276.
- Alex Renda, Yishen Chen, Charith Mendis, and Michael Carbin. 2020. DiffTune: Optimizing cpu simulator parameters with learned differentiable surrogates. In *2020 53rd Annual IEEE/ACM International Symposium on Microarchitecture (MICRO)*. IEEE, 442–455.
- Helge Rhodin, Nadia Robertini, Christian Richardt, Hans-Peter Seidel, and Christian Theobalt. 2015. A versatile scene model with differentiable visibility applied to generative pose estimation. In *Proceedings of the IEEE International Conference on Computer Vision*. 765–773.
- Luis Miguel Rios and Nikolaos V Sahinidis. 2013. Derivative-free optimization: a review of algorithms and comparison of software implementations. *J Global Optimization* 56, 3 (2013), 1247–1293.
- Connor Schenck and Dieter Fox. 2018. Spnets: Differentiable fluid dynamics for deep neural networks. In *Conference on Robot Learning*. PMLR, 317–335.
- Yuliy Schwartzburg, Romain Testuz, Andrea Tagliasacchi, and Mark Pauly. 2014. High-contrast computational caustic design. *ACM Transactions on Graphics (TOG)* 33, 4 (2014), 1–11.
- Liang Shi, Beichen Li, Miloš Hašan, Kalyan Sunkavalli, Tamy Boubekeur, Radomir Mech, and Wojciech Matusik. 2020. Match: differentiable material graphs for procedural material capture. *ACM Trans. Graph.* 39, 6 (2020), 1–15.
- Sergey Shirobokov, Vladislav Belavin, Michael Kagan, Andrei Ustyuzhanin, and Atılım Gunes Baydin. 2020. Black-box optimization with local generative surrogates. *Proc. NeurIPS* 33 (2020), 14650–14662.
- Ping Tat Sin, Hiu Fung Ng, and Hong Va Leong. 2021. Neural Proxy: Empowering Neural Volume Rendering for Animation. In *Proc. Pacific Graphics*. 1–6.
- James C Spall. 1992. Multivariate stochastic approximation using a simultaneous perturbation gradient approximation. *IEEE Trans Automatic Control* 37, 3 (1992), 332–41.
- Joe Staines and David Barber. 2013. Optimization by Variational Bounding. In *ESANN*.
- Hyung Ju Suh, Max Simchowitz, Kaiqing Zhang, and Russ Tedrake. 2022b. Do differentiable simulators give better policy gradients?. In *International Conference on Machine Learning*. PMLR, 20668–20696.
- Hyung Ju Terry Suh, Tao Pang, and Russ Tedrake. 2022a. Bundled gradients through contact via randomized smoothing. *IEEE Robotics and Automation Letters* 7, 2 (2022), 4000–4007.
- Matthew Tancik, Pratul Srinivasan, Ben Mildenhall, Sara Fridovich-Keil, Nithin Raghavan, Utkarsh Singhal, Ravi Ramamoorthi, Jonathan Barron, and Ren Ng. 2020. Fourier features let networks learn high frequency functions in low dimensional domains. *Advances in Neural Information Processing Systems* 33 (2020), 7537–7547.
- Ethan Tseng, Felix Yu, Yuting Yang, Fahim Mannan, Karl ST Arnaud, Derek Nowrouzezahrai, Jean-François Lalonde, and Felix Heide. 2019. Hyperparameter optimization in black-box image processing using differentiable proxies. *ACM Trans. Graph.* 38, 4 (2019), 27–1.
- Ethan Tseng, Yuxuan Zhang, Lars Jebe, Xuaner Zhang, Zhihao Xia, Yifei Fan, Felix Heide, and Jiawen Chen. 2022. Neural Photo-Finishing. *ACM Trans. Graph.* 41, 6 (2022), 1–15.
- Eric Veach. 1998. *Robust Monte Carlo methods for light transport simulation*. Stanford University.
- Delio Vicini, Sébastien Speierer, and Wenzel Jakob. 2022. Differentiable signed distance function rendering. *ACM Transactions on Graphics (TOG)* 41, 4 (2022), 1–18.
- Xiaotao Wan, Joseph F Pekny, and Gintaras V Reklaitis. 2005. Simulation-based optimization with surrogate models—application to supply chain management. *Computers & chemical engineering* 29, 6 (2005), 1317–1328.
- Ronald J Williams. 1992. Simple statistical gradient-following algorithms for connectionist reinforcement learning. *Machine learning* 8 (1992), 229–256.
- Chris Wyman and Scott Davis. 2006. Interactive image-space techniques for approximating caustics. In *Proceedings of the 2006 symposium on Interactive 3D graphics and games*. 153–160.
- Jiankai Xing, Fujun Luan, Ling-Qi Yan, Xuejun Hu, Houde Qian, and Kun Xu. 2022. Differentiable Rendering using RGBXY Derivatives and Optimal Transport. *ACM Transactions on Graphics (TOG)* 41, 6 (2022), 1–13.
- Kai Yan, Fujun Luan, Miloš Hašan, Thibault Groueix, Valentin Deschaintre, and Shuang Zhao. 2023. Psdr-room: Single photo to scene using differentiable rendering. In *SIGGRAPH Asia 2023 Conference Papers*. 1–11.
- Jiaxin Zhang, Hoang Tran, Dan Lu, and Guannan Zhang. 2020. A scalable evolution strategy with directional Gaussian smoothing for blackbox optimization. *arXiv preprint (2020)*.
- Dongzhan Zhou, Xinchu Zhou, Wenwei Zhang, Chen Change Loy, Shuai Yi, Xuesen Zhang, and Wanli Ouyang. 2020. Econas: Finding proxies for economical neural architecture search. In *Proceedings of the IEEE/CVF Conference on computer vision and pattern recognition*. 11396–11404.

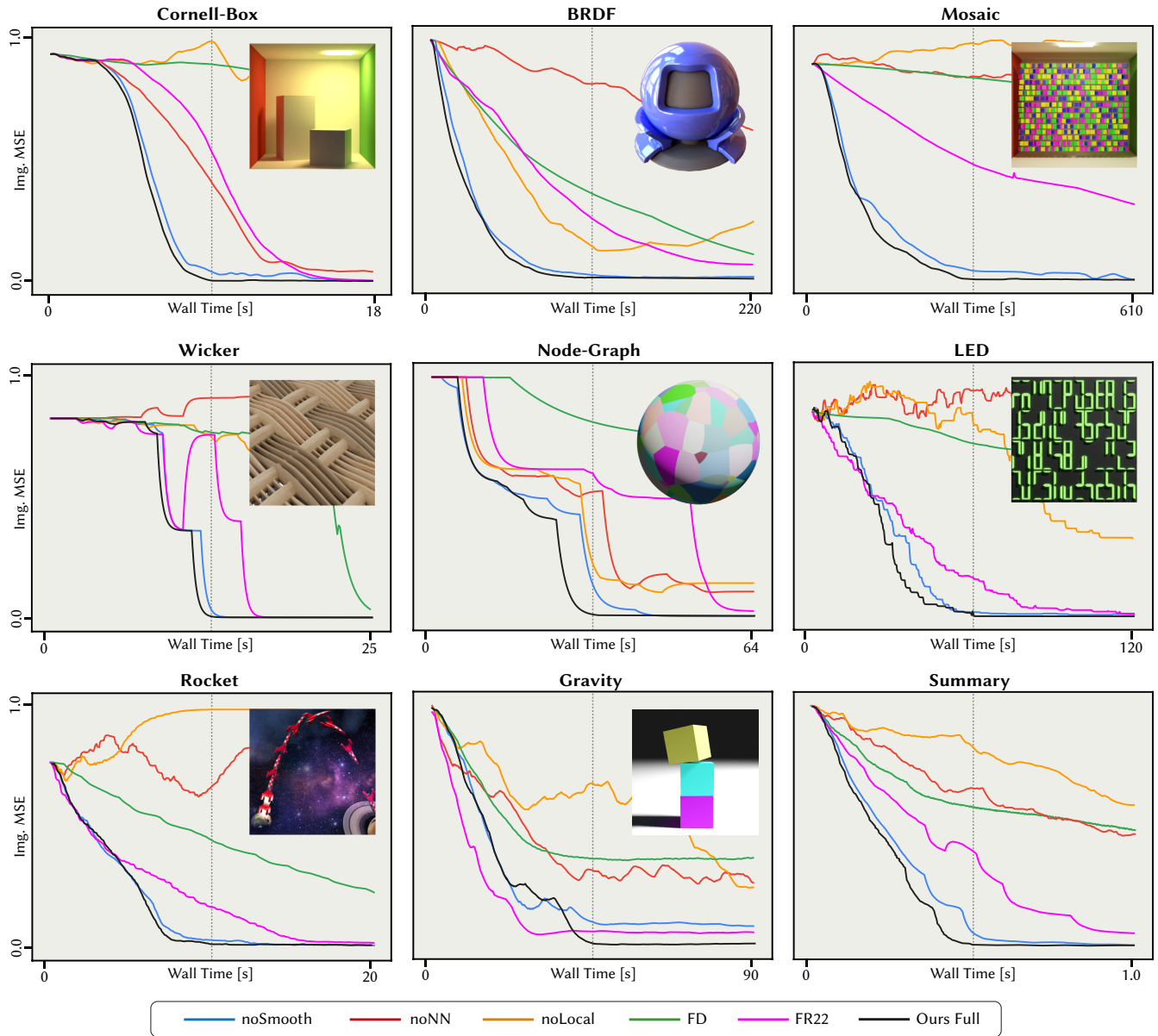


Fig. 15. We show convergence plots of all methods (wall-clock time in seconds, method colors are consistent with Tab. 2) for all tasks, ranging from differentiable rendering (top row) over procedural modelling (middle row) to animation and simulation (bottom row). For all experiments, we let our method run until convergence (the dashed vertical line in each subfigure) and then allocate *twice as much* time for the other methods to converge. All results are reported across an ensemble of 10 independent runs for all methods. For convenience, we show a summary across all tasks in the right bottom subfigure (mean across all methods, normalized and resampled). For task-specific visualizations, please see Fig. 16.

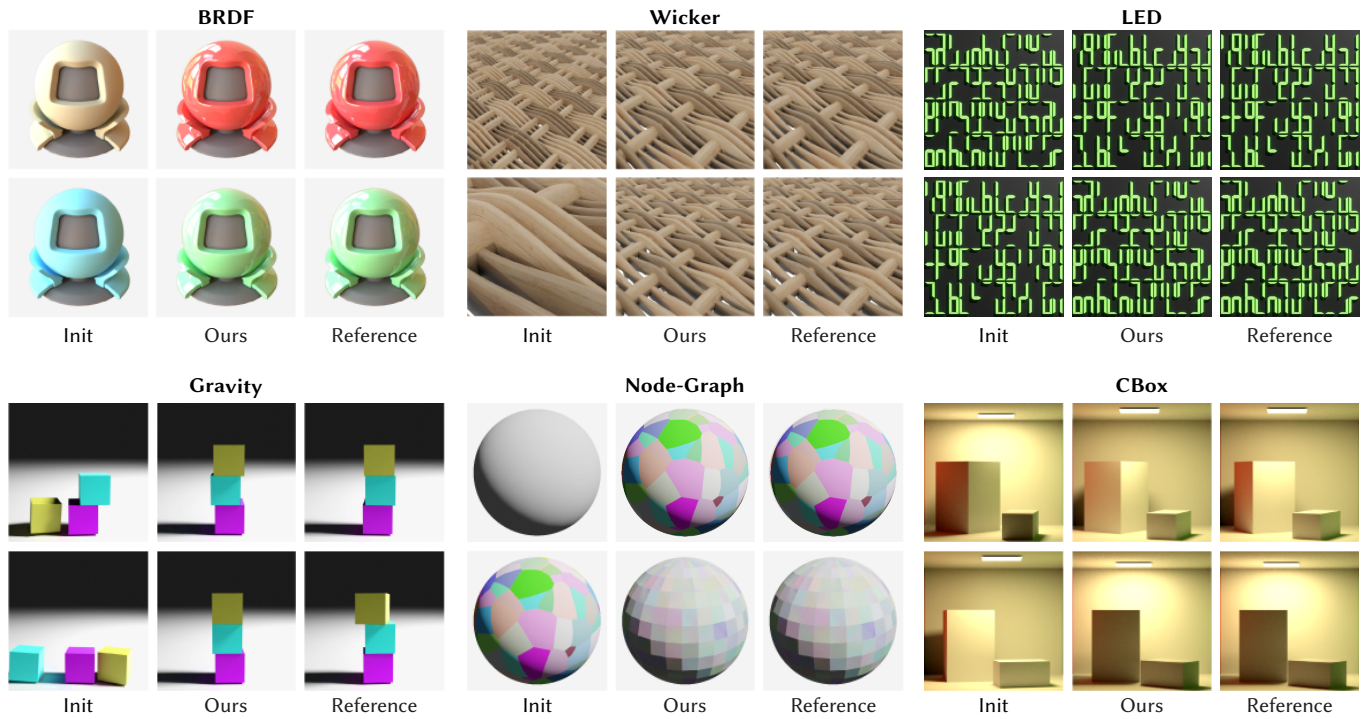


Fig. 16. Visualizations of instances of our tasks. We visualize the initial configuration in the left column of each subfigure, and our outcome and the reference in the middle and right column, respectively. For our method's convergence behaviour on these tasks, please see Fig. 15.

Zero Grads: Supplemental Materials

MICHAEL FISCHER, University College London, United Kingdom

TOBIAS RITSCHEL, University College London, United Kingdom

ACM Reference Format:

Michael Fischer and Tobias Ritschel. 2024. Zero Grads: Supplemental Materials. *ACM Trans. Graph.* 43, 4, Article 49 (July 2024), 3 pages. <https://doi.org/10.1145/3658173>

This supplementary contains additional information on our surrogate implementation and hyperparameters (Sec. 1), rendering setups (Sec. 2.1), and detailed descriptions of the tasks we solve (Sec. 2.2).

1 IMPLEMENTATION DETAILS

We implement all our experiments in PyTorch [Paszke et al. 2017]. The proxy powering our surrogate is implemented as a multi-layered perceptron (MLP) and activated by a leaky ReLU. We randomly initialize our Neural Proxy for each optimization run (via the standard PyTorch initialization, for the quadratic proxy, we choose the identity matrix) and optimize its weights alongside the parameter with a separate Adam optimizer. We perform three update steps on the surrogate parameters ϕ per optimization iteration in order to improve the surrogate’s fit to the sampled data. This is simple autodiff-driven gradient descent (GD) and hence very fast. Note that no new data is sampled between these update steps, they merely serve to improve the surrogate fit and do not increase the required computational budget. For all gradient updates, we use the Adam optimizer with standard parameters and learning rates as specified in Tab. 1. We additionally experimented with different sampling patterns and found both both low-discrepancy (Sobol) and antithetic samples and found both to improve performance, and adapt antithetic samples for simplicity. We normalize the network’s inputs to $[0,1]$. For the lower-dimensional tasks ($n_{\text{dim}} < 50$), it suffices to use 3 hidden layers with 64 neurons each, whereas for the higher-dimensional tasks (below the horizontal line in Tab. 1), we found that we needed to increase the surrogate’s capacity to 8 layers à 128 neurons and additionally use positional encoding to increase the frequencies that the network can encode.

1.1 Hyperparameters

Our method comes with two hyperparameters: the number of samples N we use to estimate our surrogate’s gradient with (cf. Alg.2 in the main text), and the spread of the locality kernel λ , which will influence how far these samples are spaced out around the current parameter θ .

Authors’ addresses: Michael Fischer, University College London, United Kingdom, m.fischer@cs.ucl.ac.uk; Tobias Ritschel, University College London, United Kingdom, t.ritschel@ucl.ac.uk.

Permission to make digital or hard copies of part or all of this work for personal or classroom use is granted without fee provided that copies are not made or distributed for profit or commercial advantage and that copies bear this notice and the full citation on the first page. Copyrights for third-party components of this work must be honored. For all other uses, contact the owner/author(s).

© 2024 Copyright held by the owner/author(s).

0730-0301/2024/7-ART49

<https://doi.org/10.1145/3658173>

Table 1. Our hyperparameters σ_o and N , as well as the experiment settings for the different tasks, sorted by dimensionality in ascending order. MPL is short for matplotlib.

	σ_o	N	n_{dim}	LR θ	LR ϕ	Renderer
WICKER	0.33	2	3	1×10^{-3}	1×10^{-3}	Blender
BRDF	0.33	2	4	1×10^{-3}	1×10^{-3}	Mitsuba
CBOX	0.10	2	4	5×10^{-4}	1×10^{-3}	Mitsuba
GRAVITY	0.20	2	5	1×10^{-3}	1×10^{-3}	Blender
ROCKET	0.33	2	10	1×10^{-3}	5×10^{-4}	MPL
NODEGR.	0.20	2	24	1×10^{-3}	1×10^{-3}	Blender
LED	0.33	2	336	1×10^{-3}	1×10^{-3}	Blender
MOSAIC	0.025	16	320	5×10^{-4}	1×10^{-3}	Blender
CAUSTIC	0.013	20	1,024	2×10^{-4}	1×10^{-4}	PyTorch
MESH	0.025	20	7,686	2×10^{-3}	1×10^{-4}	NVDiff.
SPLINE GEN.	0.025	20	8,764	1×10^{-5}	1×10^{-4}	MPL
MLP	0.025	20	35,152	1×10^{-4}	1×10^{-4}	MPL
TEXTURE	0.025	20	196,608	1×10^{-5}	1×10^{-4}	MPL

We specify the number of samples N we use for estimating the surrogate’s gradients in Tab. 1. For the lower-dimensional tasks, it suffices to use $N = 2$, whereas for the higher-dimensional tasks, the noise and higher variance from this rough gradient estimate impede convergence and thus require higher sample counts. We would like to emphasize that those are still far lower than what competing methods use, e.g., $2n_{\text{dim}}$ for finite differences (FD) or $m \times n_{\text{dim}}$, $m \gg 2$, for directional Gaussian smoothing (DGS) [Zhang et al. 2020]. Our method also benefits from more samples in the lower-dimensional regime, but these come at the cost of increased compute, which is why we tried to achieve a minimal number to keep the overhead low.

We show a comparison of different sample counts on the **MESH** and **MLP** tasks in Fig. 3 and detail the remaining hyperparameters and experiment settings in Tab. 1, where σ_o denotes the spread of the locality kernel λ . As a general rule of thumb, we recommend setting the initial σ_o to 0.33 on normalized domains and finetune from there, if necessary. For higher-dimensional, interlinked problems, we have found a more fine-granular sampling to be necessary and use $\sigma_o = 0.025$. We use 15% of the locality spread as the spread of the smoothing kernel κ .

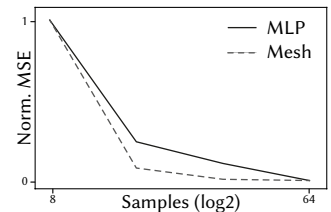


Fig. 3. Final error vs. samplecount N .

2 TASKS

This section provides information on the task setup, problems, goals and rendering architectures used.

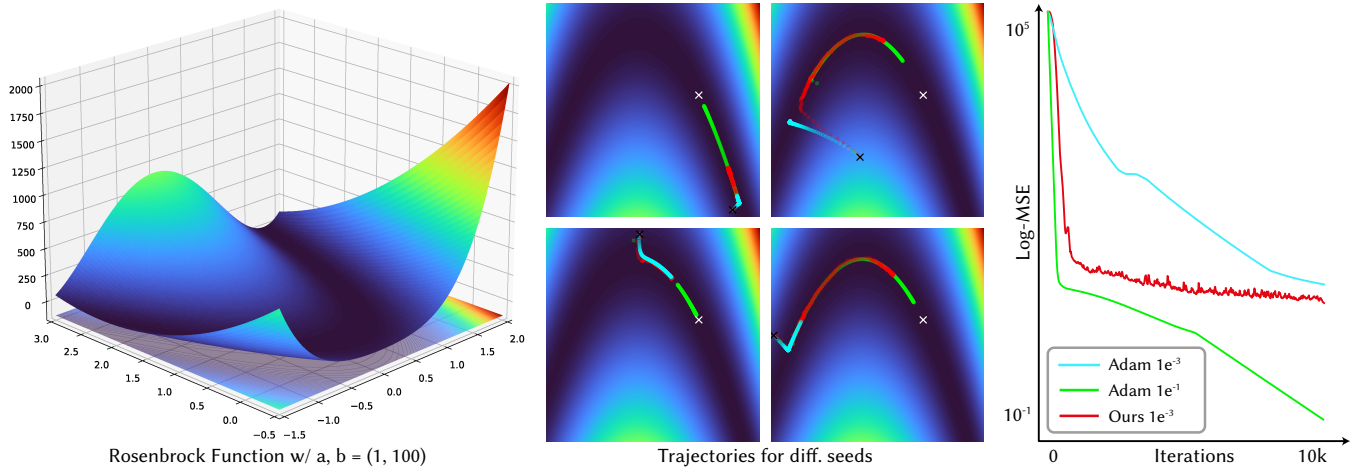


Fig. 1. We evaluate our method on the Rosenbrock function against gradient descent with analytical gradients and Adam with equal learning rate, sample count and iterations. Similar to Adam, our method struggles to make progress in the valleys of low slope, a common limitation of gradient-based techniques. Adam, with a higher learning rate, converges faster than our method. The convergence plots in the right subfigure are median values over an ensemble of 10 independent runs and seeds.

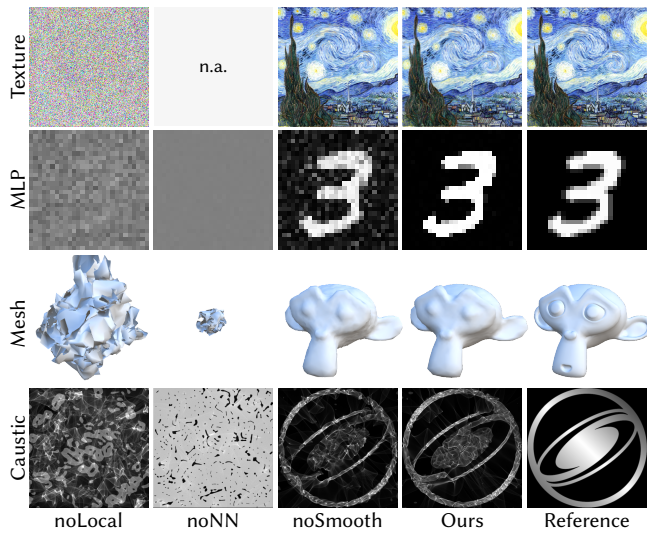


Fig. 2. We show the results of our ablated methods from the main manuscript (Sec. 4.1) on the higher-dimensional tasks. Similar to CMA, the result for the quadratic proxy (noNN) could not be run due to the quadratic memory complexity.

2.1 Rendering

To render the images for the tasks Mosaic, Wicker, LED, NodeGraph and Gravity, we interface our method with Blender via an efficient socket-based local TCP network, which enables us to make use of Blender’s rendering engines and the embedded physics solver. All images were set to render noise-free under either Eevee or Cycles, with 16 to 128 samples and denoising activated. For the tasks BRDF and Cornell-Box, and the comparisons with Mitsuba, we use Mitsuba 3 [Jakob et al. 2022] with the path-replay backpropagation integrator at 16spp. For the Mesh task, we use NVDiffRast [Laine

et al. 2020] with standard hyperparameters. For the remaining tasks Rocket, Spline Generation and Texture, we use a custom matplotlib-based renderer [Hunter 2007]. Note that none of this interfacing is necessary for our method to work, but pure convenience for rapid prototyping and reducing I/O times from and to disk. Most importantly, we do not propagate any gradient information through the rendering process, even if this were possible, e.g., when using a differentiable renderer. One could alternatively render an image, save it to disk and manually load it and perform a gradient update step, which would yield the same results, but be arguably less convenient.

2.2 Task Descriptions

2.2.1 Higher Dimensions. While some of our higher-dimensional example tasks could in theory also be solved via established, specialized methods (e.g., [Holl et al. 2020; Jakob et al. 2022; Nicolet et al. 2021]), they show that our method scales well to higher dimensional problems and reinforce our argument of general applicability. All comparisons to the following optimization algorithms are performed under the same budget of function evaluations.

For the comparisons with genetic algorithms (GAs), we use the publicly available Python package pygad [Gad 2021]. For simulated annealing (SA) [Xiang et al. 2013], we use the scipy library [Virtanen et al. 2020]. For simultaneous perturbation stochastic approximation (SPSA) [Spall 1992], we use the publicly available spsa package [Nguyen 2022]. Note that, while we use standard hyperparameters for the other packages, we here adapted the SPSA perturbation radius to the sampling radius used by our method in order to enable a fair comparison (the default value of 2.0 is too large for many of our problems, e.g., for the delicate task of network training).

TEXTURE For the **TEXTURE** task, we use our method to optimize the 256 pixels of an image texture, leading to a $256 \times 256 \times 3 = 196,608$ optimization problem. We randomly initialize the texels from $\mathcal{N}(0.5, 0.05)$, i.e., they are drawn from a Normal distribution

with mean 0.5, corresponding to a grey value. As is common, we additionally employ a whitening transform during optimization [Nimier-David et al. 2019].

MLP This task is an extension of the texture task to address the concern that optimization variables are not sufficiently interlinked with each other. To this end, we train a MLP to replicate randomly sampled digits from the MNIST [LeCun 1998] dataset. The MLP has two ReLU-activated hidden layers of 32 neurons and a final layer with 784 neurons that is activated by a Sigmoid, leading to a total of 35,152 network weights and hence to a 35,152-dimensional optimization problem. The weights are initialized via the standard formula $\mathcal{U}(-k, k)$, where k is the reciprocal of the layer’s input features [Paszke et al. 2017].

CAUSTIC For this task, we take inspiration from Wyman and Davis [2006] and write a fast, rasterization-based caustic renderer.

The idea is that a parallel bundle of rays from a far-away directional light source hits a parameterized refractive surface (our heightfield, usually modeled as a glass slab [Nimier-David et al. 2019; Pappas et al. 2011; Schwartzburg et al. 2014]), and gets refracted according to Snell’s law (we use an index of refraction of 1.33). The refracted rays then hit a receiver plane, where we record, for each pixel, the number of received rays, resulting in an approximate caustic. We use an equal ray- and receiver resolution of 512p. The relation between the optimization variables (the heightfield, in our case parameterized as a cubic B-Spline of resolution 32^2 , randomly initialized) and the final output in this task is highly non-linear, as a change in the heightfield has the potential to affect various pixels across the entire receiver plane. Moreover, the task is not trivially differentiable, as the conversion of the (continuous) hitpoint on the receiver plane to discrete pixel coordinates in the image grid is a discontinuous operation.

MESH For the **MESH** task, we optimize the vertices of a triangle mesh such that the renderings of the mesh match those of a reference shape. Our source mesh has 2,562 vertices whose 3D positions we optimize, leading to a highly interlinked 7,686-dimensional problem. We follow the approach in [Nicolet et al. 2021] and use their smooth formulation, the AdamUniform optimizer and the Laplacian regularization, thereby nicely showing that our surrogate successfully learns to replicate the regularized loss landscape. For fairness, all competitors operate in this parametrization. Following [Nicolet et al. 2021], the source shape is initialized as a tessellated sphere and rendered from 13 different viewpoints under environment illumination using NVDiffRast [Laine et al. 2020] – however, without backpropagating their gradient information; all gradients employed in the optimization are produced by our surrogate.

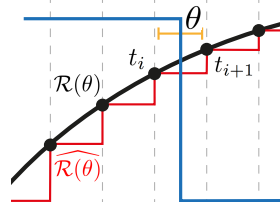


Fig. 4. An illustration why differentiating an ODE solver $\mathcal{R}(\theta)$ w.r.t. time is not trivially differentiable: moving the event-time θ of the blue signal within the yellow interval will not affect the observed outcome, as the solver operates on the discretized version $\hat{\mathcal{R}}$ only and will continue to observe “on” and “off” at timesteps i and $i + 1$, respectively.

SPLINE GENERATION For the **SPLINE GENERATION** task, we train a generative model, a variational autoencoder (VAE)[Kingma and Welling 2013], to replicate digits from the MNIST dataset in a spline representation. Our VAE consists of an encoder-MLP with roughly 40k neurons, and a decoder-MLP with 8,764 neurons. To stabilize training, we use a pre-trained encoder that serves as feature extractor and projects the MNIST images into the latent space, from where we learn a generative decoder that predicts the horizontal and vertical translation of 10 spline support points (initialized diagonally across the image plane). Subsequently, we fit a spline through these predicted support points with a (matplotlib-based) non-differentiable renderer and learn our surrogate on the reconstructed splines’ image-space mean-squared error (MSE), regularized by the VAE’s Kullback-Leibler divergence (KLD) (weighting factor 0.1). Descending along the surrogate gradients then produces the weights for a generative decoder that can be sampled to generate new MNIST digits. Again, we initialize all stateful components with the standard formula $\mathcal{U}(-k, k)$, where k is the reciprocal of a layer’s input features [Paszke et al. 2017].

REFERENCES

- Ahmed Fawzy Gad. 2021. PyGAD: An Intuitive Genetic Algorithm Python Library. *arXiv:cs.NE/2106.06158*
- Philipp Holl, Vladen Koltun, and Nils Thuerey. 2020. Learning to control pdes with differentiable physics. *arXiv preprint arXiv:2001.07457* (2020).
- J. D. Hunter. 2007. Matplotlib: A 2D graphics environment. *Computing in Science & Engineering* 9, 3 (2007), 90–95. <https://doi.org/10.1109/MCSE.2007.55>
- Wenzel Jakob, Sébastien Speierer, Nicolas Roussel, Merlin Nimier-David, Delio Vicini, Tizian Zeltner, Baptiste Nicolet, Miguel Crespo, Vincent Leroy, and Ziyi Zhang. 2022. Mitsuba 3 Renderer, 2022.
- Diederik P Kingma and Max Welling. 2013. Auto-encoding variational bayes. *arXiv preprint arXiv:1312.6114* (2013).
- Samuli Laine, Janne Hellsten, Tero Karras, Yeongho Seol, Jaakko Lehtinen, and Timo Aila. 2020. Modular primitives for high-performance differentiable rendering. *ACM Transactions on Graphics (TOG)* 39, 6 (2020), 1–14.
- Yann LeCun. 1998. The MNIST database of handwritten digits. <http://yann.lecun.com/exdb/mnist/> (1998).
- Jack Nguyen. 2022. spsa. <https://github.com/SimpleArt/spsa>.
- Baptiste Nicolet, Alec Jacobson, and Wenzel Jakob. 2021. Large Steps in Inverse Rendering of Geometry. *ACM Transactions on Graphics (Proceedings of SIGGRAPH Asia)* 40, 6 (Dec. 2021). <https://doi.org/10.1145/3478513.3480501>
- Merlin Nimier-David, Delio Vicini, Tizian Zeltner, and Wenzel Jakob. 2019. Mitsuba 2: A Retargetable Forward and Inverse Renderer. *Transactions on Graphics (Proceedings of SIGGRAPH Asia)* 38, 6 (Dec. 2019). <https://doi.org/10.1145/3355089.3356498>
- Marios Pappas, Wojciech Jarosz, Wenzel Jakob, Szymon Rusinkiewicz, Wojciech Matusik, and Tim Weyrich. 2011. Goal-based caustics. In *Computer Graphics Forum*, Vol. 30. Wiley Online Library, 503–511.
- Adam Paszke, Sam Gross, Soumith Chintala, Gregory Chanan, Edward Yang, Zachary DeVito, Zeming Lin, Alban Desmaison, Luca Antiga, and Adam Lerer. 2017. Automatic differentiation in pytorch. (2017).
- Yuliy Schwartzburg, Romain Testuz, Andrea Tagliasacchi, and Mark Pauly. 2014. High-contrast computational caustic design. *ACM Transactions on Graphics (TOG)* 33, 4 (2014), 1–11.
- James C Spall. 1992. Multivariate stochastic approximation using a simultaneous perturbation gradient approximation. *IEEE Trans Automatic Control* 37, 3 (1992), 332–41.
- Pauli Virtanen, Ralf Gommers, Travis E Oliphant, Matt Haberland, Tyler Reddy, David Cournapeau, Evgeni Burovski, Pearu Peterson, Warren Weckesser, Jonathan Bright, et al. 2020. SciPy 1.0: fundamental algorithms for scientific computing in Python. *Nature methods* 17, 3 (2020), 261–272.
- Chris Wyman and Scott Davis. 2006. Interactive image-space techniques for approximating caustics. In *Proceedings of the 2006 symposium on Interactive 3D graphics and games*. 153–160.
- Yang Xiang, Sylvain Gubian, Brian Suomela, and Julia Hoeng. 2013. Generalized simulated annealing for global optimization: the GenSA package. *R J.* 5, 1 (2013), 13.
- Jiaxin Zhang, Hoang Tran, Dan Lu, and Guannan Zhang. 2020. A scalable evolution strategy with directional Gaussian smoothing for blackbox optimization. *arXiv preprint* (2020).